STRUCTURAL INFLUENCE ON THE EVOLUTION OF A PRE-EONILE DRAINAGE SYSTEM OF SOUTHERN EGYPT: INSIGHTS FROM MAGNETOTELLURICS AND GRAVITY DATA

By

JEFFREY DALE RODEN

Bachelor of Science in Geology

Oklahoma State University

Stillwater, Oklahoma

2011

Submitted to the Faculty of the
Graduate College of the
Oklahoma State University
in partial fulfillment of
the requirements for
the Degree of
MASTER OF SCIENCE
May, 2011

STRUCTURAL INFLUENCE ON THE EVOLUTION OF A PRE-EONILE DRAINAGE SYSTEM OF SOUTHERN EGYPT: INSIGHTS FROM MAGNETOTELLURICS AND GRAVITY DATA

Thesis Approved:

Dr. Estella Atekwana

Thesis Adviser

Dr. Eliot Atekwana

Dr. Alex Simms

Dr. Mark E. Payton

Dean of the Graduate College

ACKNOWLEDGMENTS

The completion of this thesis would not be possible without the assistance of Dr. Estella Atekwana, Dr. Eliot Atekwana, Dr. Alex Simms, and Dr. Mohamed Abdel Salam. I am forever grateful for your guidance and assistance throughout my graduate and undergraduate degrees. I would especially like to thank Dr. Estella Atekwana for giving me the opportunities to travel abroad. These are experiences that I will never forget. I would also like to thank all the faculty and staff of the Oklahoma State University Geology department.

This thesis project was made possible through funding from the National Science Foundation International Research Experiences for Students. I would like to thank Dr. Gad El-Qady for his assistance with the Stratagem during my field work in Egypt and his continued assistance in processing the data upon returning home. I also extend my gratitude to Leslie Lansbery and Ali Atef for contributing their research, South Valley University in Aswan for their logistical support, and all the undergraduate and graduate students from Alexandria University-Damanhour, Sohag University, and Missouri S&T for their help in the field.

I would like to thank my biggest supporter, my father, for always being there for me and the assistance he provided me for my education. I would like to dedicate this thesis to my mother, you are forever missed. I would also like to thank my fiancée Maggie Silvertooth for all of her encouragement and support.

TABLE OF CONTENTS

LIST OF TABLES

Table Page

LIST OF FIGURES

Figure Page

Figure Page

Figure Page

CHAPTER I

INTRODUCTION

The relative roles of tectonics and climate in shaping the Earth's landscape have received significant attention. However, many questions remain unanswered, such as what role pre-existing structures have in controlling the landscape and if these pre-existing structures are the most important factor in controlling topographic evolution. The Nile River provides a unique opportunity to examine tectonic processes and climate continuously shaping the dynamic surface of the Earth (Goudie, 2005). The Egyptian Nile, the northernmost segment of the Nile River, is particularly important to answering some of these questions because it contains a record of over 20 Ma of geologic history displaying the relationship between evolving drainage systems, regional tectonics (the opening of the Red Sea and the subsequent uplifting of the Red Sea Hills), local structures (Cretaceous and younger faulting), and climate change (the Messinian Salinity Crisis and the emergence of the Sahara) (Abdelsalam et al., 2000; Gani et al., 2007; Stern and Abdelsalam, 1996; Thurmond et al., 2004).

Predating the onset of the modern Nile, which started ~6 Ma ago with the Eonile phase (Said, 1993), numerous rivers flowed from the east across the Eastern Sahara until a major change in climate desiccated the area (Figure 4) (Ghoneim et al., 2007). The presence of ancient river channels was unknown until 1981 when images from NASA's Shuttle Imaging Radar Mission (SIR-A) revealed numerous channels buried beneath the sand shedding light on the

fluvial past of the Sahara. Since the discovery much debate has centered on the age of the abandoned channels (Ghoneim et al., 2007; McCauley et al., 1986; McCauley et al., 1982). Several researchers, (Issawi and McCauley, 1992; McCauley et al., 1986), suggest the origins of these drainage systems to begin in the Late Eocene while others, (Butzer and Hansen, 1968; El Bastawesy et al., 2010; Ghoneim et al., 2007; Said, 1993), consider them to be relics from the Early to Middle Pleistocene.

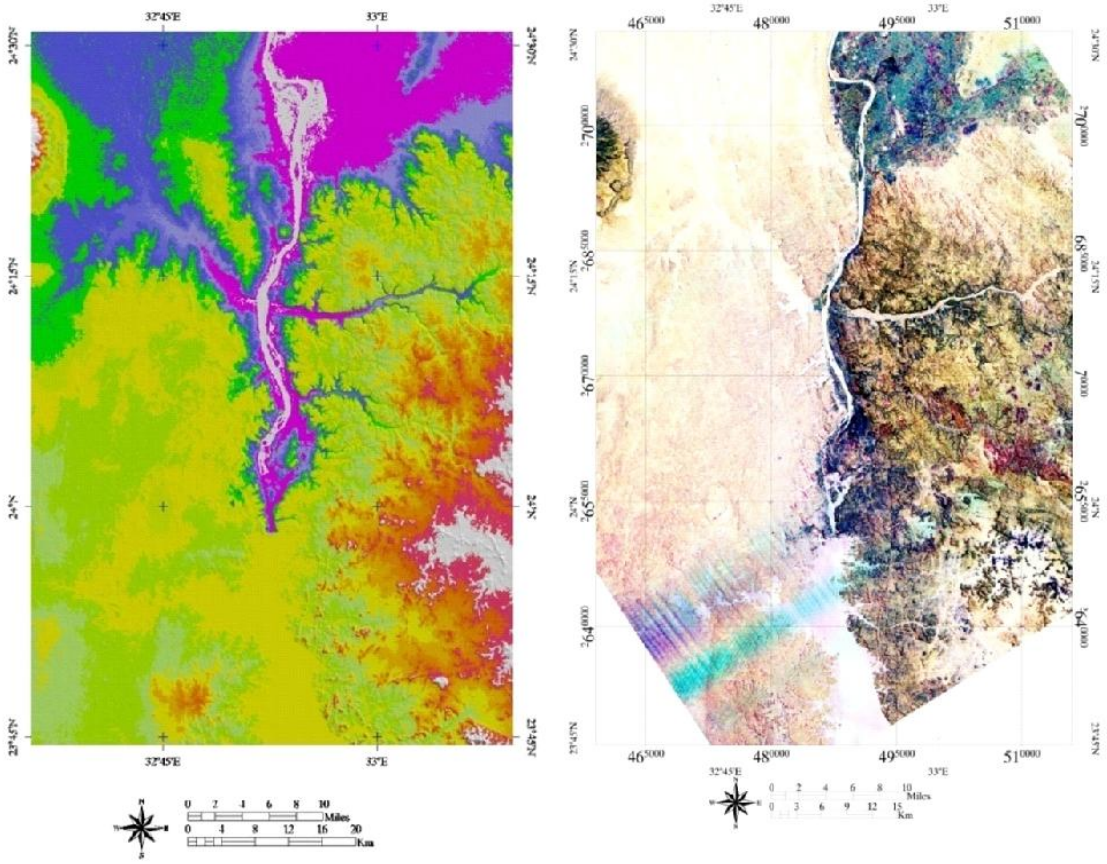

Figure 1: (A) Shuttle Radar Topography Mission (SRTM) Digital Elevation Model (DEM) of southern Egypt showing geomorphological features of the study area. The DEM suggests that the Modern Nile course was superimposed on the Wadi Abu Subeira – Wadi Kobbania drainage system which was once flowing from east to northwest. (B) 1/Lhv-1/Lhh-1/Chv Shuttle Imaging Radar (SIR)-C image enhanced though synthetic coloring. The image shows the details of Wadi Kobbania drainage system (because of radar penetration of the Sahara sand). The image suggests that the northwest flowing Wadi Kobbania might have ended forming an internal delta.

The Wadi Kobbania and the Wadi Abu Subeira are two of these abandoned paleodrainages located in southern Egypt (Figure 1 and Figure 2). The Wadi Kobbania has been interpreted by several researchers as serving as the downstream continuation of the Wadi Abu Subeira forming a W to NW flowing river that existed prior to the modern Nile River. It can be traced as far north as the Gallaba Plain where it becomes obscured by the Quaternary gravel and sand deposits (Butzer and Hansen, 1968; El Bastawesy et al., 2010; Ghoneim et al., 2007; Hinz et al., 2003). The Wadi Abu Suberia – Wadi Kobbania paleodrainage system was just one of many westerly flowing rivers sourced from the east by uplift of Precambrian crystalline rocks of the Red Sea Hills driven by the rifting of the Red Sea in the Oligocene. The sharp turn from a westerly flow to the northwest is potentially due to the presence of a NW trending fault influencing the flow path of the stream.

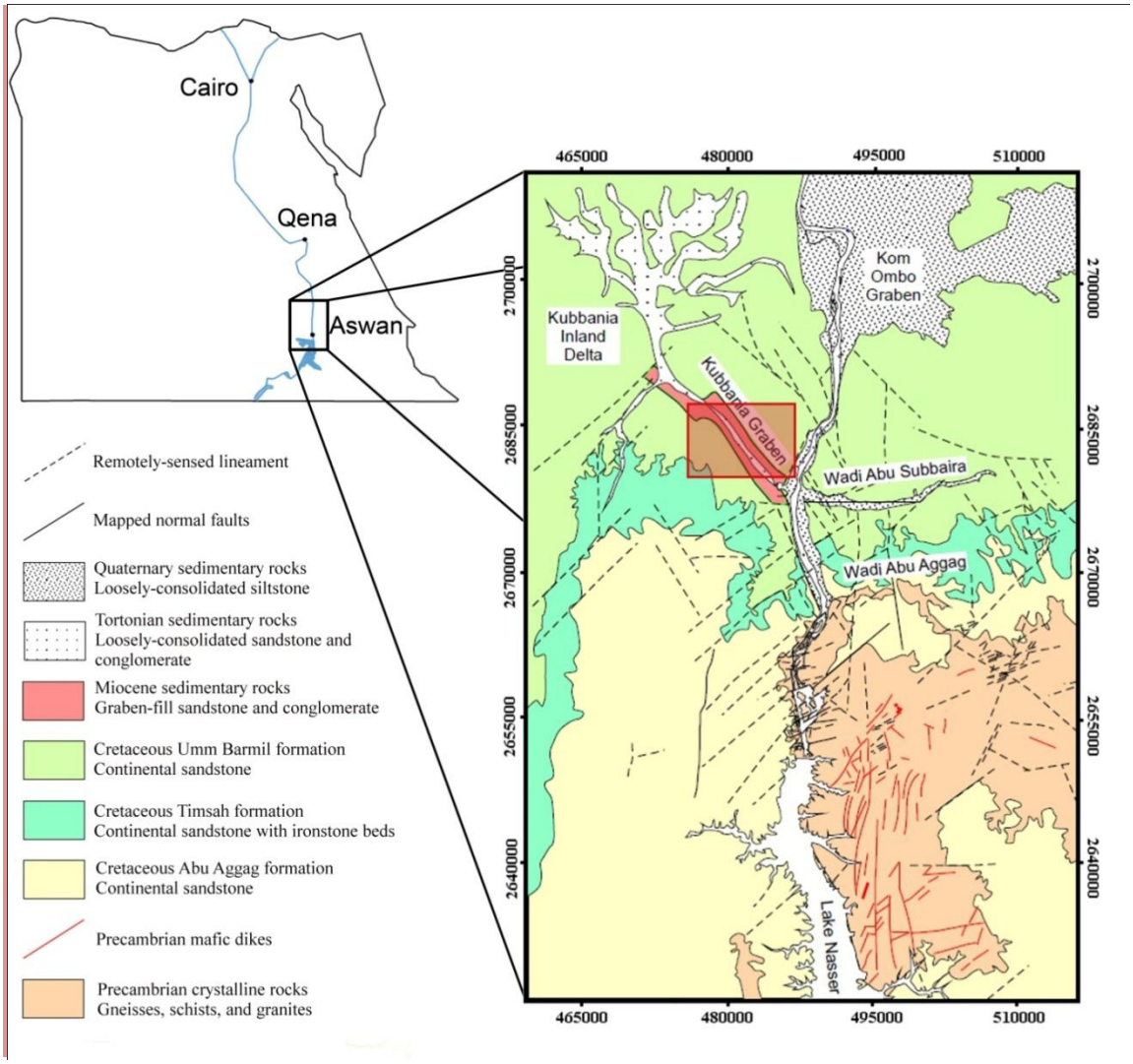

Figure 2: Geologic map of area around the city of Aswan. Red shaded square indicates the study area in Wadi Kobbania seen in Figure 7 and Figure 8. Map modified from Lansbery (2010).

This study was initiated as part of a US National Science Foundation (NSF) International Research Experience for Students (IRES) funded project. The study focuses on using two geophysical techniques, magnetotellurics (MT) and gravity, along with the geologic history of southern Egypt in order to test the following hypotheses: (1) The Wadi Abu Subeira – Wadi Kobbania drainage system represents a Pre-Eonile phase of a river system that flowed from the Red Sea Hills of the Eastern Desert of Egypt and (2) that the spatial distribution of the drainage related to the Pre-Eonile phase is controlled by NW-trending faults forming the Wadi Kobbania graben. Understanding ancient paleochannels such as the Wadi Kobbania is important, as they are promising locations to explore for groundwater as recharge from the Nile may still occur, especially if the alluvial base is located at an elevation lower than the modern Nile. Also, understanding the paleodrainage is useful for determining the effect of regional tectonics and local structure on the drainage system predating the modern Nile.

1.1 Geologic Setting

Fluvial systems within Africa are relatively young, with many of the major rivers changing dramatically since the disintegration of Gondwanaland in the Cretaceous (Goudie, 2005). The Nile River is no exception. The Nile is the lifeblood of Egypt and holds the title of the longest river in the world, flowing through ten different countries and spanning close to 7,000 km and draining 3.2 million km^2 watershed (Goudie, 2005). The Nile flows through five regions differing from one another in geologic history and structure: the great Lake Plateau of Central Africa, the Sudd and Central Sudan, Ethiopian Highlands, the Cataract Nile, and finally the Egyptian Nile ending at the Nile delta at the Mediterranean Sea (Goudie, 2005; Said, 1981). The dating of the first appearance of fertile soil transported to the Egyptian Nile Valley from the Ethiopian Plateau and Equatorial Africa has shown that the Egyptian Nile did not connect with the sub-Sahara Africa Nile System until ~800 ka (Said, 1993). Said (1981; 1993) has classified the evolution of the modern Egyptian Nile River into 7 stages beginning in the late Miocene

~6 Ma with what he termed the "Eonile phase". The Eonile period was controlled by the Messinian Salinity Crisis, when the desiccation of the Mediterranean Sea resulted in carving a ~1000 km long, ~300 m deep canyon stretching in a north-south direction from the Nile Delta to the present day city of Aswan (Krijgsman et al., 1999). The remaining 6 stages of the evolution of the modern Nile are outlined in Figure 3.

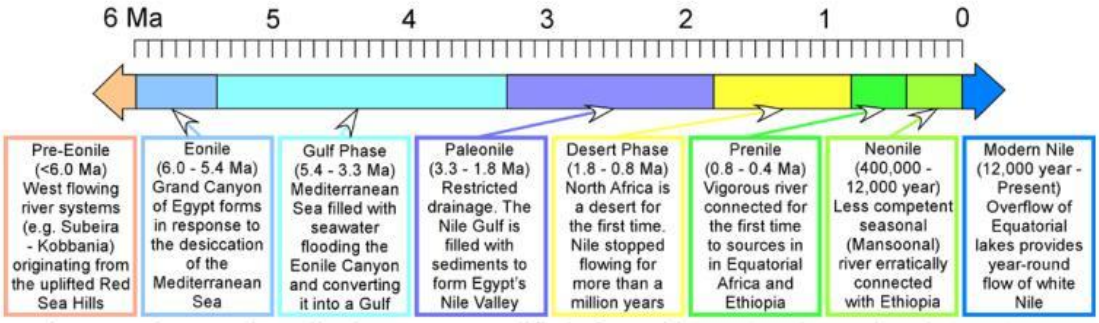

Figure 3: A timeline depicting the different stages contributing to the evolution of the modern Nile River. Compiled from Said (1981; 1993).

Egypt is located in northeastern Africa and is composed of four major provinces: the Nile Valley and Delta, the Western Desert, the Eastern Desert, and the Peninsula of Sinai. The study area is located along the Nile Valley close to the city of Aswan. The geology of Aswan is unique in that it contains outcropping Precambrian crystalline rocks overlain by Cretaceous-aged Nubian Sandstone formations. The two rocks units are separated by an almost sub-horizontal unconformity. The Precambrian rocks in Aswan composed of quartzofeldspathic schists and gneisses containing biotite, hornblende, and almandite-garnet representing green schist to amphibolite facies metamorphic products of volcanic arc systems which were developed during the Neoproterozoic Pan African event ultimately resulting in the formation of the Arabian-Nubian Shield (Gindy and Tamish, 1998; Morgan, 1990; Youssef, 2003). These rocks show well-developed NW-trending planar fabrics and folds, most likely related to the NW-trending, sinistral Najd fault system. These layered rocks are intruded by unmetamorphosed and undeformed

granitoid rocks. The Nubian Sandstone constitutes three clastic formations: the Abu Aggag, Timsah, and the Umm Barmil (El Naggar, 1970; Tawardros, 2001). The three formations represent a transgression of the Tethys Sea between two regressive phases (Attia, 1955; Kerdany and Cherif, 1990). The Abu Aggag was deposited via braided fluvial river systems in the Turonian and lies nonconformably on top of the Precambrian crystalline rocks with a thickness of ~40 m or more in the city of Aswan and thickening to the north and northeast (Hendriks et al., 1990; Kerdany and Cherif, 1990; Klitzsch and Squyres, 1990; Tawardros, 2001). During the Coniacian, the Timsah was deposited conformably over the Abu Aggag in a shallow marine environment reaching a thickness of 5-50 m and contains oolitic iron ore deposits that were actively mined in Aswan until the early 1970's (Attia, 1955; Hendriks et al., 1990; Klitzsch and Squyres, 1990; Tawardros, 2001). Lacustrian and fluvial deposition resulted in the Umm Barmil Formation attaining a thickness of 15-50 m during the early Campanian (Attia, 1955; Hendriks et al., 1990; Klitzsch and Squyres, 1990; Tawardros, 2001). In the Aswan area the Nubian Sandstone reaches a maximum thickness of ~160 m (Youssef, 2003).

This study is focused on the Wadi Kobbania in the Western Desert of southern Egypt. The Wadi Kobbania is located 15 km north of Aswan and terminates on the eastern end at the modern Nile River and is the main wadi on the pediplain surface (Wendorf and Schild, 1976). Research has been focused on Wadi Kobbania due to its sudden northwesterly deflection possibly indicating the presence of a northwest-trending structure that controls the course of this ancient river. It has been postulated that incision of the wadi is ~5 m near the Nile River and increasing in depth to the west to a maximum of ~40 m in the middle of the wadi (Wendorf and Schild, 1976). This wadi is bounded to the northeast and southwest by subtle plateaus where the Umm Barmil Formation (which is the uppermost formation of the Nubian Sandstone) is exposed at the surface indicating that the other Nubian Sandstone formations are present in the subsurface.

Geological observations from shallow trenches (~10 m deep) within the wadi indicate that at least the upper part of Wadi Kobbania is filled with loosely consolidated coarse sandstone and conglomerate with a dominance of Precambrian crystalline rock clasts coming from the Red Sea Hills, which represent part of the Nubian Shield. Based on their regional setting, Lansberry (2011) suggested that these sediments are Miocene in age.

Issawi and McCauley (1992) suggests that during the Cenozoic Era, Egypt was likely drained by at least three different major drainage systems which formed in response to tectonic uplifts and sea-level changes spanning the Late Eocene; the retreat of the Tethys Sea, to the Late Pleistocene; the beginning of the modern Nile. Issawi and McCauley (1992) termed these three stages the "Gilf System" (40 to 20 Ma), the "Qena System" (24 to 6 Ma), and the "Nile System" (6 Ma to present). The paleodrainage system of Wadi Abu Subeira-Wadi Kobbania began during the Gilf system, developing due to uplift in the Red Sea Hills, and lasted through the Qena System. The paleodrainage eventually evolved into one of many active alluvial river systems in the Tortonian (~11 Ma) and lasted until the start of the Nile system. Issawi and McCauley (1992) suggested that the Nile system is characterized by a regression of the Mediterranean Sea in the Late Miocene epoch. This large regression known as the Messinian Salinity Crisis was caused by uplift under the Strait of Gibraltar, cutting off the only connection the Mediterranean Sea had to the world's oceans, converting the sea into a great lake (Said, 1993). The desiccation of the isolated sea caused a rapid drop in base level of more than 1000 m creating a large N-S trending valley rivaling the size of the Grand Canyon. The creation of this massive Nile Canyon resulted in the truncation of the Wadi Abu Suberia-Wadi Kobbania paleodrainage (Figure 4). This truncation also resulted in a drainage reversal of Wadi Kobbania, which now drains in a SE direction into the modern Nile River. The Messinian Salinity Crisis is also used by Said (1981; 1993) to mark the beginning of the "Eonile" system.

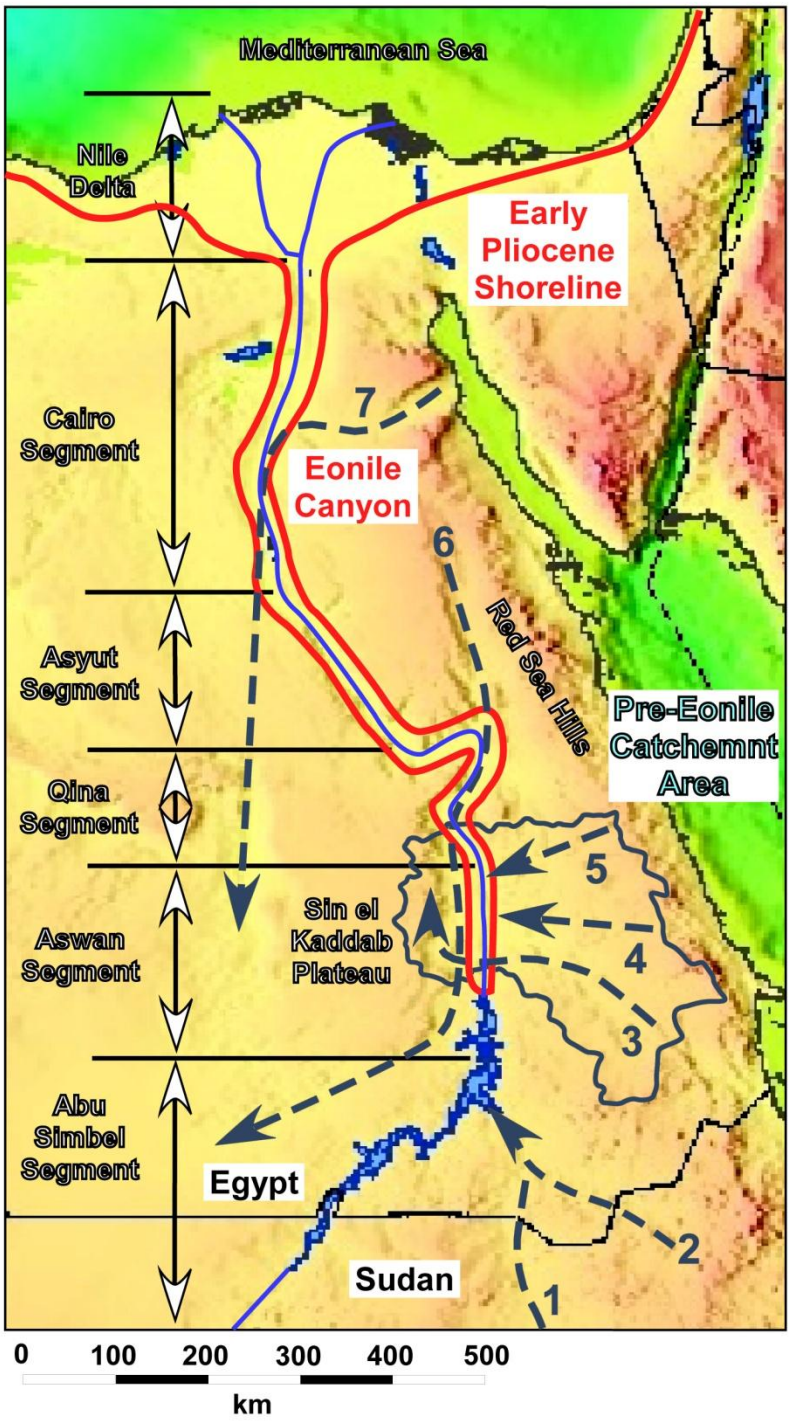

Figure 4: Digital Elevation Model (DEM) of Egypt showing the Pliocene shoreline, the extent of the Eonile Canyon, Pre-Eonile catchment area, and major paleo-rivers. (1) Wadi Gabgaba; (2) Allaqi; (3) Wadi Abu Subeira–Wadi Kobbannia; (4) Wadi Shait –Wadi Natash; (5) Wadi Abad; (6) Wadi Gena–Radar Rivers; (7) Tarfa. Taken from (Lansbery, 2010).

1.2 Structural Setting

Egypt is structurally divided into 3 regions: the stable shelf, the unstable shelf, and the Arabian-Nubian Shield (Figure 5) (Meshref, 1990). The Arabian-Nubian Shield has the most clearly defined and agreed upon boundaries (Youssef, 2003). The Arabian-Nubian Shield is represented by the uplifted, and subsequently exposed, Precambrian crystalline rocks of the southern Sinai Peninsula and Red Sea Hills. The stable shelf covers the largest portion of the country and surrounds the Arabian-Nubian Shield. The stable shelf's origins lie with Egypt undergoing a period of relative tectonic quiescence during the Paleozoic era after enduring the intense magmatic and tectonic events of the Pan African Orogeny in the Neoproterozoic. This period of tectonic quiescence, along with the denudation of the Pan African highlands from glaciations, allowed for the peneplanation of the surface, which allowed widespread transgression and deposition of marine facies beginning in the Late Cretaceous (Morgan, 1990; Youssef, 2003). The unstable shelf dominates most of northern Egypt and is defined by severe rock deformation due to rapid basin subsidence from tectonism and wrench faulting from the closing of the Tethys Sea (Youssef, 2003).

Egypt has 7 main tectonic trends, which vary in strength and prevalence throughout the country (Figure 5): north-south (Nubian trend); north-northeast (Aqaba trend); east-west (Tethyan trend); west-northwest (Darag trend); east-northeast (Syrian Arc trend); northeast (Tibesti trend), and northwest (Red Sea trend) (Meshref, 1990). The east-west Tethyan trend, i.e. the Kalabsha fault, and the northwest Red Sea trend are the dominant fault trends in the Aswan area.

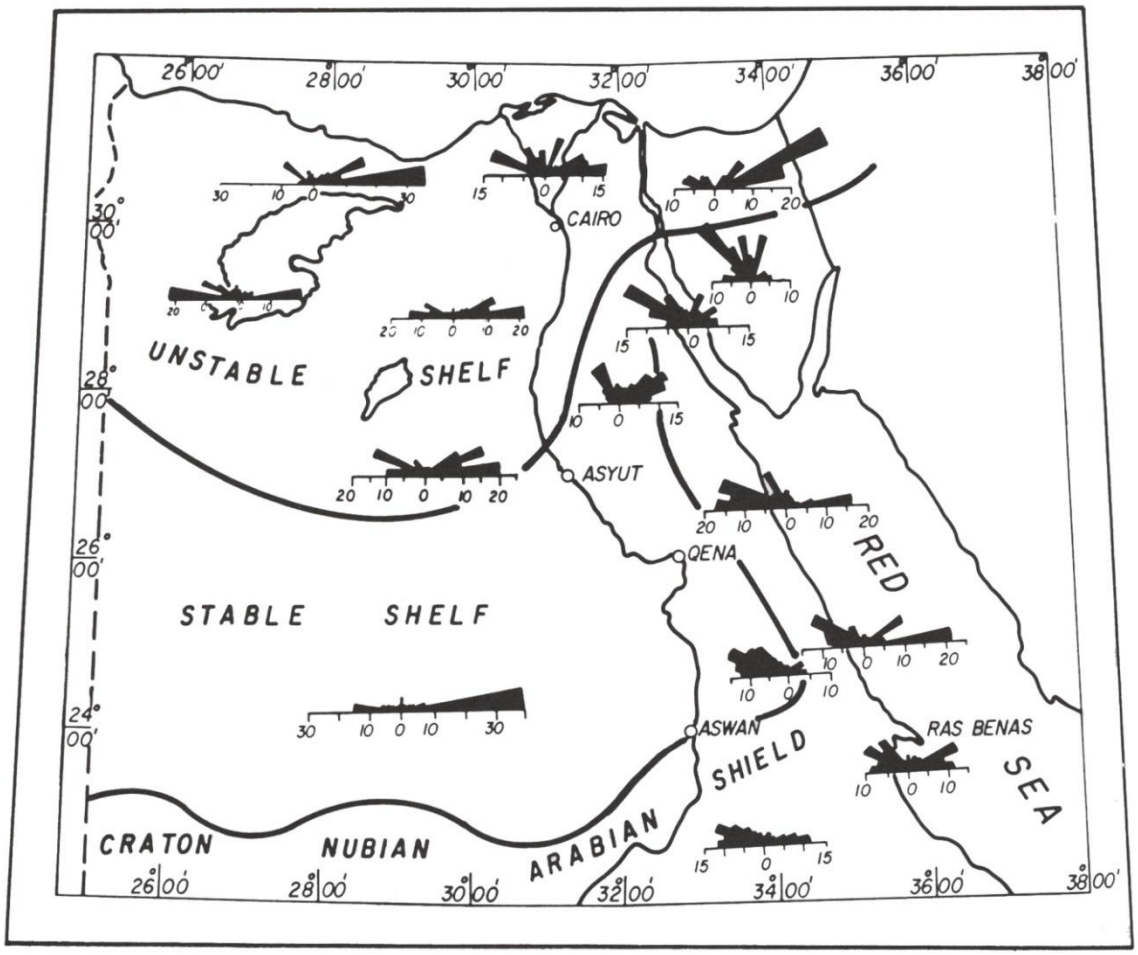

Figure 5: Rosetta diagrams showing the major tectonic trends of Egypt and the approximate boundaries of the unstable shelf, stable shelf, and Arabian Nubian Shield (Meshref, 1990).

The east-west Tethyan trend formed during the Paleozoic and part of the Mesozoic as the African continent was uplifted. As Pangea began to break up during the Mesozoic, uplifting throughout most of Egypt came to an end (Klitzsch and Squyres, 1990). Controversy surrounds much of the origins of the structural features formed during the Mesozoic but there is general agreement that it was a period of major extensional tectonics (Morgan, 1990). The two main tectonic forces were sinistral shearing during the late Jurassic to early Cretaceous, then a

transition to dextral shearing until the Paleocene, as North Africa collided with Laurasia (Meshref, 1990). Nelson (1986) postulated that Mesozoic tectonics resulted from extensional wrench faulting acting on the preexisting east-west Tethyan trend, as well as re-activation of the older Precambrian trends.

Rifting of the Red Sea and the subsequent uplift of the Red Sea Hills began during the lower Oligocene ~30 Ma as the Arabian plate separated with an anticlockwise rotation from North Africa (Makris et al., 1991; Morgan, 1990; Tawardros, 2001). The position of the Red Sea itself, and its subsequent grabens, had already been established ~600 Ma during the Neoproterozoic as a zone of structural weakness resulting from either a suture zone or from wrench faulting during the Pan-African Orogeny (Harris and Gass, 1981; Makris et al., 1991; Tawardros, 2001; Youssef, 1968). Ancestral rivers predating the modern Nile originated at the same time this rifting was initiated (Said, 1981). The Aswan area is affected by many faults dating from the Cretaceous trending E-W, N-S, NE and NW (Figure 2). The majority of these faults are normal and dextral strike-slip faults, which displace Precambrian crystalline rocks, Late Cretaceous Nubian Sandstone and shale, Late Cretaceous shale of the Dakhla Formation, and Paleocene limestone of the Kurkur, Garra, and Dungul Formations (EGSMA, 1981; Issawi, 1969).

CHAPTER II

METHODS

Two geophysical methods, magnetotellurics (MT) and gravity, were used to image the sub-surface structure of the Wadi Kobbania using a Stratagem EH-4 hybrid MT system and a CG-5 gravimeter. Data were acquired over 14 days of field work conducted during the first half of January 2010. These data were collected with the help of American and Egyptian graduate and undergraduate students from: Oklahoma State University, Missouri S&T, Sohag University, and Alexandria University-Damanhur. The MT and gravity methods were chosen due to the limitations imposed upon other EM and geophysical techniques by the sandy environment, time available for field work, and desired depth of penetration (> 400 m). The gravity method and the EH-4 Stratagem also collect data along large traverses in a relatively short amount of time due to quick set up and rapid acquisition of data.

In addition to the geophysical methods, two sand samples were collected from the middle of the wadi and used to determine the conductivity and major ion concentrations. Pre-weighed samples (31.5 mg and 30.7 mg) were each placed into 50 ml of 18Ω deionized water in a centrifuge tube and mechanically shaken for 24 hours. Samples were then centrifuged at 4500 rpm for 15 minutes to separate out the solids. The conductivity and total dissolved solids of an aliquot of the supernatant was measured by microelectrode. In addition the Cl^-, SO_4^{-2}, Ca^{+2}, Mg^{+2}, K^+ and Na^+ were measured by ion chromatography and the bicarbonate content by sulfuric acid titration.

2.1 MT Method

The Magnetotelluric method is a natural-source electromagnetic technique that acquires surface measurements of orthogonal time-varying electric and magnetic fields, which are then used to determine subsurface conductivity and the geoelectric structure of the Earth (Cagniard, 1953). The natural signals used by the MT method typically range from 10^4 to 10^{-4} Hz (Vozoff, 1991). Energy signals below 1 Hz are generated by solar winds moving through the Earth's magnetosphere and ionosphere, the very same energy that causes the aurora borealis phenomenon at high latitudes (Jones, 1993; Vozoff, 1991). The Stratagem unit is not designed to register lower frequency waves generated from solar plasma, but rather measures soundings at a higher frequency range, resulting in shallower depth imaging. Signals measured above 1 Hz are a resultant of lightning storms transmitting their energy through the Earth's ionosphere and can be generated from up to half the globe away (Jones, 1993; Vozoff, 1991). Due to the high conductivity contrast of the air-earth boundary, the law of refraction states that the electromagnetic waves will be refracted vertically into the Earth upon penetration regardless of their incidence angle (Telford et al., 1990).

Equation 1: $n_1 sin\theta_1 = n_2 sin\theta_2$

Where θ_1 and θ_2 are angles from the normal of the incident and refracted waves and n_1 and n_2 are the refractive indices of the medium the waves travel through. These propagating primary electromagnetic waves will then generate eddy currents in conductors within the subsurface, in turn generating secondary magnetic fields measured at the surface. The amplitude and phase of the electric fields being measured depends on the conductivity of the medium that the fields travel through, and will differ from the primary incident electromagnetic field in phase, magnitude, and direction (Bedrosian, 2007).

Electromagnetic energy propagating through the earth begins to decay exponentially as it penetrates deeper into the subsurface. This decrease in signal is known as the skin effect. The skin depth can be used to calculate how deep the signal will penetrate before attenuating to 1/e of its original value at the surface of the conducting body. Assuming a homogenous earth, skin depth (δ) is controlled by the resistivity of the earth (ρ) and the frequency ($\omega=2\pi f$) of the incident field shown in equation 2, μ is the magnetic permeability.

Equation 2: $\delta = \sqrt{\frac{2\rho}{\mu\omega}} \approx 500\sqrt{\frac{\rho}{f}}\text{meters}$

It can be seen from the equation that lower frequency signals and/or higher resistivity will result in a greater depth of penetration into the earth.

Observed magnetotelluric data are transformed to the frequency domain at which the electric field, E, and the magnetic field, H, are linearly related with each other,

Equation 3: $\begin{bmatrix} E_x \\ E_y \end{bmatrix} \begin{bmatrix} Z_{xx} & Z_{xy} \\ Z_{yx} & Z_{yy} \end{bmatrix} \begin{bmatrix} H_x \\ H_y \end{bmatrix}$

The element, Z, comprises the magneotelluric impedance tensor, and is generally complex due to phase differences between electric and magnetic fields. Once the electrical and magnetic fields are measured, apparent resistivity and phase can be calculated from the impedance tensor using Cagniard's formula (Cagniard, 1953):

Equation 4: $\rho_{xy} = \frac{1}{\omega\mu_0}\left|Z_{xy}\right|^2, \varphi_{xy} = \tan^{-1}\left[Z_{xy}(\omega)\right]$

Equation 5: $\rho_{yx} = \frac{1}{\omega\mu_0}\left|Z_{xy}\right|^2, \varphi_{yx} = \tan^{-1}\left[Z_{yx}(\omega)\right]$

where ω is the angular frequency and μ_0 denotes the permeability of free space (H/m).

When dealing with 2D datasets, the 2D observed impedance tensor, Equation 6, will be composed of two zeros at a diagonal and the two terms at the off diagonal will be different from one another. One term is the X (Z_{xy}) direction and represents current flowing along geological strike, the other term is the Y (Z_{yx}) direction and represents the current flowing across the strike. This results in generating two sounding curves. The X direction will generate what is known as the Transverse Electric (TE) mode, Equation 7. The Y direction generates the Transverse Magnetic (TM) mode, Equation 8.

Equation 6: $Z_{obs} = RZ_{2D}R^T = R\begin{bmatrix} 0 & Z_{xy} \\ Z_{yx} & 0 \end{bmatrix}R^T$

Equation 7: $E_x(\theta) = Z_{xy}H_y(\theta)$

Equation 8: $E_y(\theta) = Z_{yx}H_x(\theta)$

Rocks are poor conductors. Therefore, current flow is usually due to fluid filling their pore spaces. This type of current flow is known as electrolytic conduction and is predominantly controlled by the conductivity of the fluid contained within these pores. Conductivity is also affected to a lesser degree by the volume and arrangement of the pores in the rock. Archie's Law is an expression of this statement.

Equation 9: $\rho_e = a\phi^{-m}{S_w}^{-n}\rho_w$

where ρ_e is bulk resistivity, ρ_w is resistivity of the pore filling fluid, ϕ is fractional pore volume, S_w is saturation, m is the cementation factor if the rock, n is the saturation exponent, and a is the tortuosity factor.

2.2 MT Data

MT data were collected along two profiles, shown in Figure 7, across Wadi Kobbania using a Geometrics EH-4 Stratagem Unit. This unit is capable of measuring electrical resistivity to depths of a few meters to more than 1km. The Stratagem system is unique in that it uses both natural and man-made electromagnetic signals. Thus it is not a pure MT system, but rather a "hybrid" MT system blending together both natural source magnetotellurics (MT) and controlled source audio-frequency magnetotellurics (CSAMT). The Stratagem uses natural signals in all measured frequency ranges. However, natural signals are generally weak in the higher frequency range. The Stratagem solves this problem by using artificial signals generated from a transmitter to "boost" the weak natural signal at these higher frequencies. The Stratagem unit measures electrical and magnetic field changes in the frequency range of 100 KHz to 11.7 Hz.

To acquire soundings, the Stratagem was assembled at each station with a 50 m dipole length in the X and Y directions using 4 buffered electrodes with stainless steel stakes (Figure 6). The location of profile 1 was chosen due to the existence of an abandoned road which crosses and runs almost perpendicular to Wadi Kobbania. The profile was 5.2 km in length and comprised of 28 stations with a 250 m station spacing. The start of the second profile was ~3 km SE of profile 1 and was 5 km in length with 19 stations spaced at 250 m. The Y direction dipole was oriented 315° and the X dipole 225° in order to keep the X dipole parallel to the geologic strike direction.

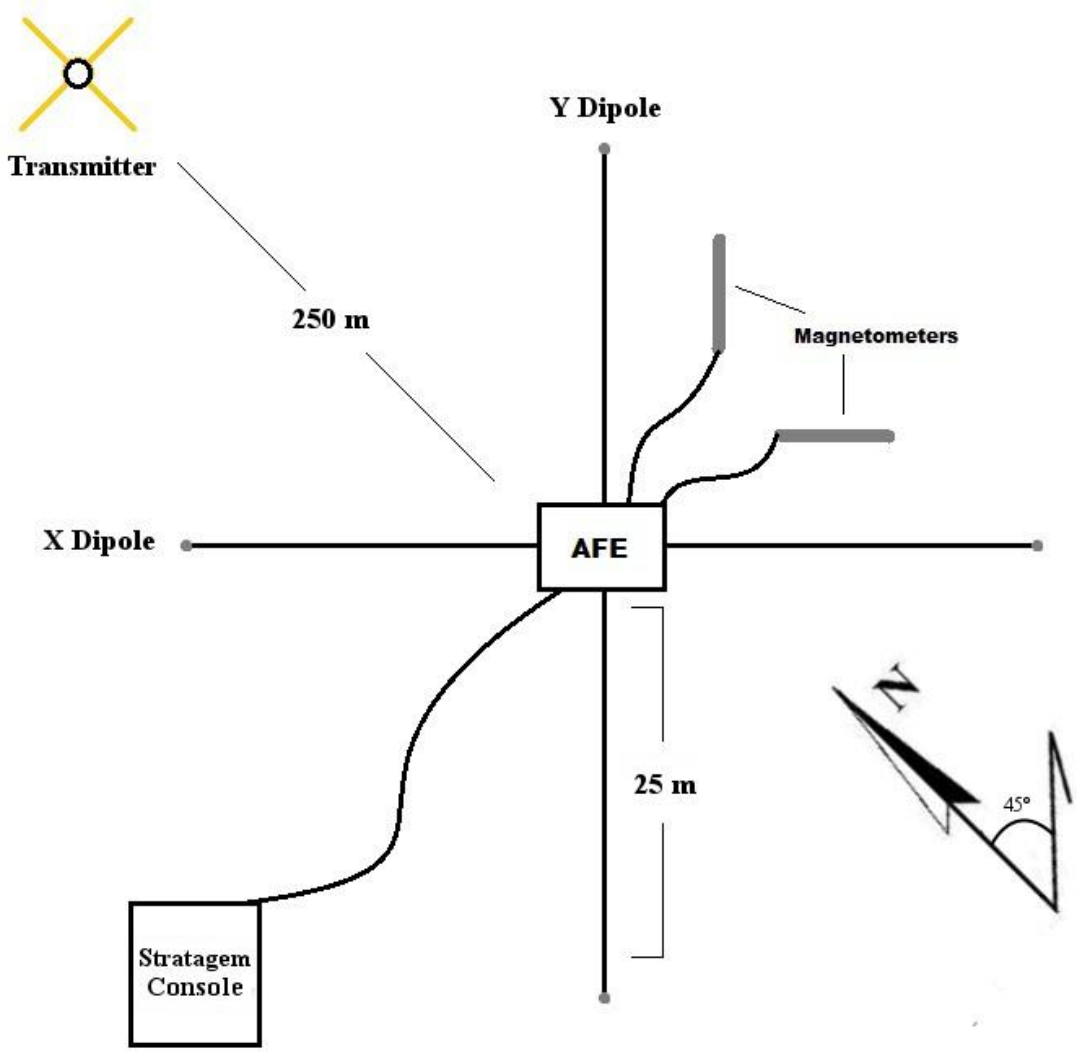

Figure 6: Schematic detailing field setup of the EH4-Stratagem unit. Y dipole was rotated 45° from north in order to keep perpendicular to geologic strike. Transmitter used for high frequency acquisition was placed 250 m from the Acquisition Front End (AFE).

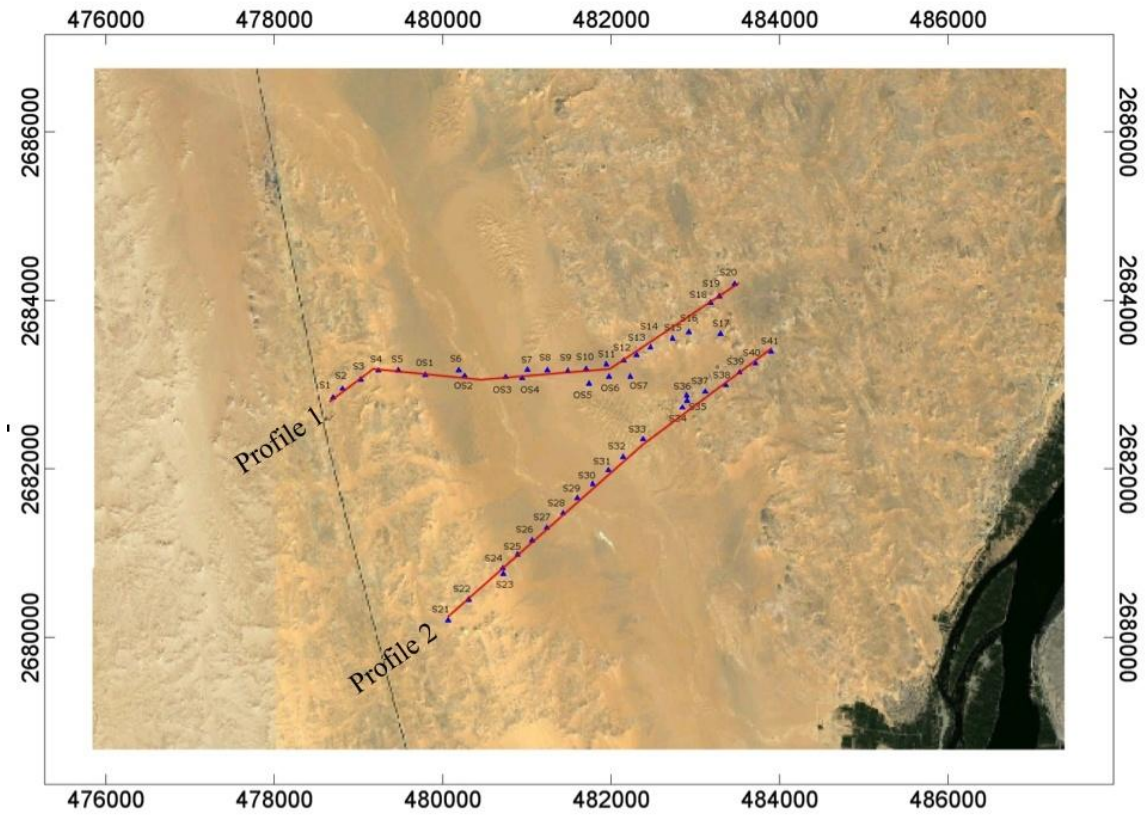

Figure 7: Profile 1 and Profile 2 MT showing station locations across Wadi Kobbania at a 250 m station spacing, Poor contact or hard terrain required some stations to be offset or moved closer to one another.

2.3 Gravity Method

The gravity method is an attractive geophysical tool in that acquiring data is quick and can be used over any type of terrain regardless of culture interference due to it being a passive instrument. The gravimeter measures the relative change in gravity between a base station and an observation station. Corrections are applied to account for variations in gravity due to instrument drift, gravitational pull of the moon, latitude, elevation, and excess mass from variations in elevation. Standard gravity, the natural gravitational force exerted by the Earth, is ~980.665 mGal, any difference between it and the corrected gravity readings are attributed geologic structures.

2.4 Gravity Data

Gravity data were collected over 62 stations across the Wadi Kobbania using a Scintrex CG-5 Gravimeter and a TopCon GPS system to record accurate elevations. The gravity measurements were carried out along the same direction and orientation of MT profile 1, but with a 100 m station spacing to provide higher resolution (Figure 8). Many stations were measured repeatedly in order to assess reliability of readings. After acquisition the data were processed to correct for variations in gravity resulting from differences in elevation, latitude, and topography. The average crustal density of 2.67 g/cm^3 was used as the slab density for the Bouguer correction. All gravity readings are relative to the base station only and were not tied to a known absolute gravity base station. The gravity data acquired over the study site is presented in Appendix I.

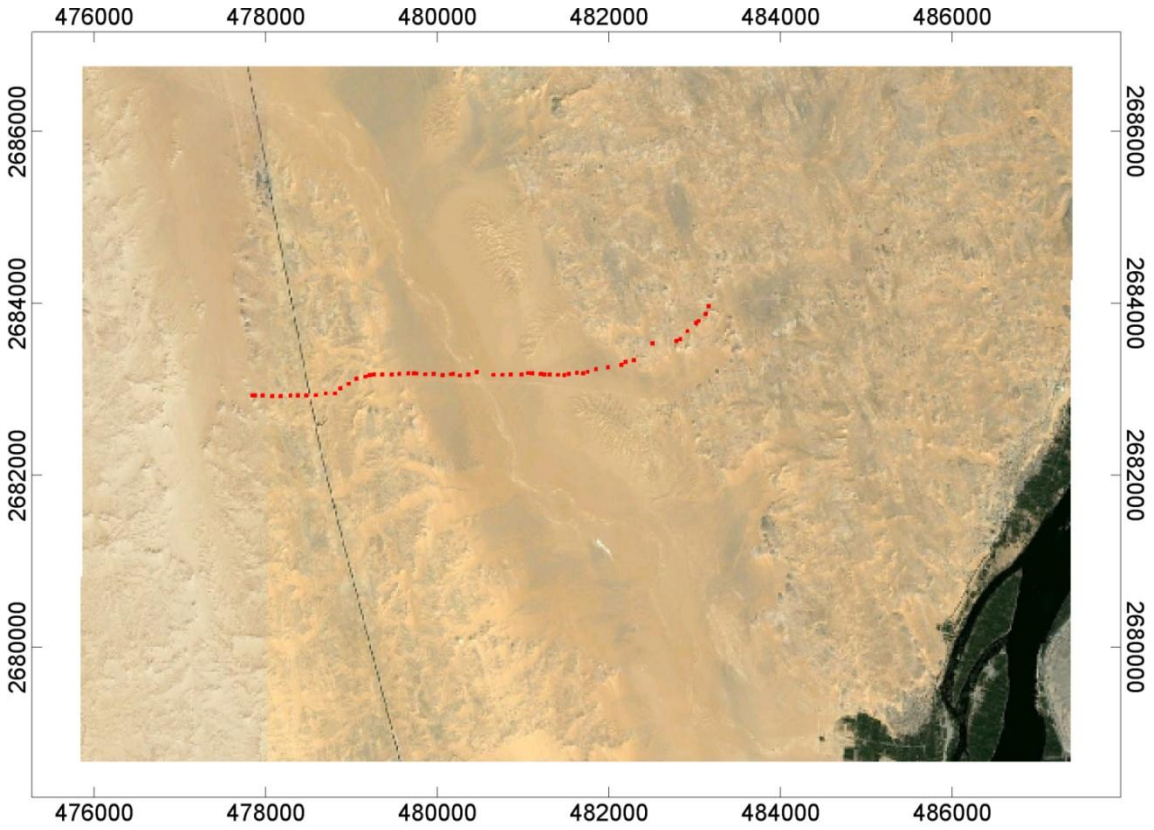

Figure 8: Station locations for Gravity profile spaced 100 m apart across Wadi Kobbania.

Samples from each formation of the Nubian Sandstone: Umm Barmil, Timsah, Abu Aggag as well as the Precambrian crystalline basement were collected in the field. The Umm Barmil samples were cut into 27 billets, Timsah into 19 billets, Abu Aggag into 12 billets and Precambrian rock into 11 billets. Each billet of rock was then weighed to determine its mass and subsequently inserted into a graduated cylinder filled with water to measure the amount of water displaced to determine its volume. The density was then calculated by taking the mass divided by the volume. All measured sample data is found in Appendix II. The average density results for each formation are displayed in Table 1. The average density was taken across the three different sandstone formations of the Nubian Sandstone resulting in an average of 2.4 g/cm^3. The derived densities were then used for the gravity model created in GYM-SYS in Geosoft's Oasis Montaj software package.

Average Umm Barmil Density	Average Timsah Density	Average Abu Aggag Density	Average Precambrian Crystalline Rock Density
2.69 g/cm^3 ±9.0%	2.38 g/cm^3 ±5.7%	2.13 g/cm^3 ±18.1%	2.62 g/cm^3 ±4.9%

Table 1: Average densities and relative standard deviations measured from formation samples obtained from the Aswan area.

2.5 Data Processing

Cultural influence posed problems due to a high tension power line running ~300 m to the west of station1 and 1 km to the west of profile 2. Other factors leading to poor data quality in the stations were very dry yet conductive sand, which made it difficult in obtaining good contact between the ground and the electrodes. To overcome this problem, bentonite rich mud

from the Nile River banks was collected and mixed with salt water and then poured into the electrode holes.

All data were acquired during the daytime between 10 A.M. to 5 P.M. The MT data are of better quality when acquired at night but due to safety and logistics this was not possible. Finally, Egypt itself lies within an MT deadband zone as can be seen in Figure 9, showing worldwide distribution of lightning strikes which the MT method relies upon. All of these factors lead to a dataset containing scattered impedances for soundings at some stations.

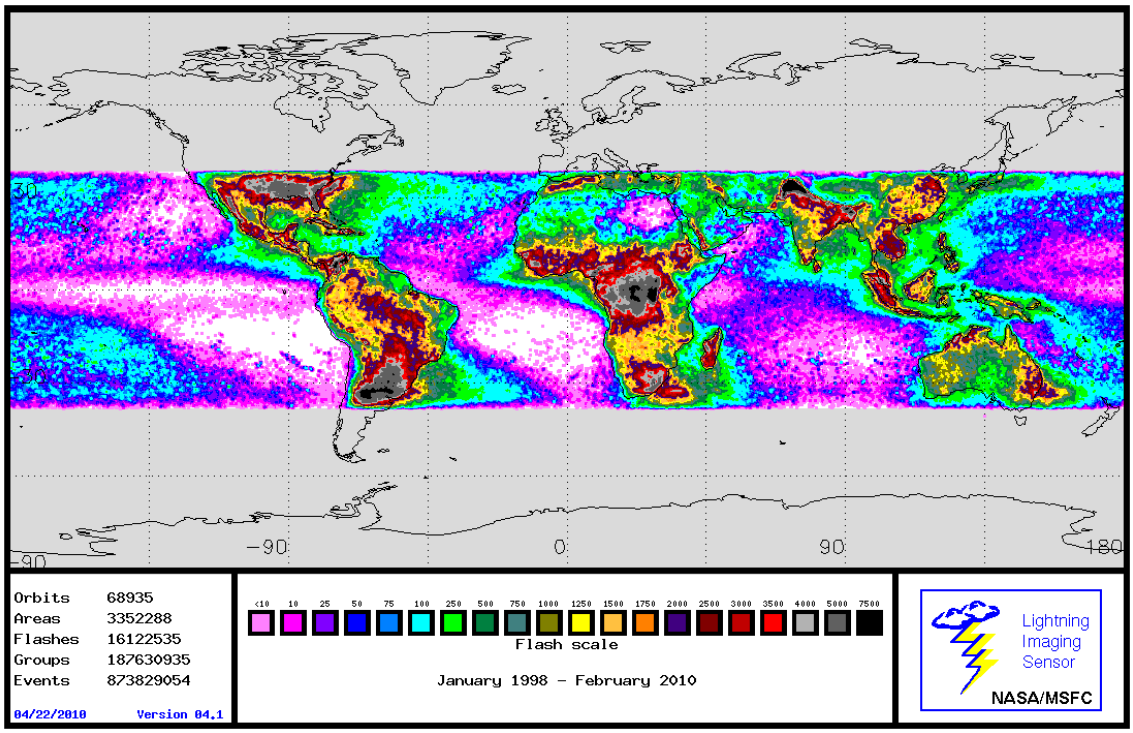

Figure 9: Distribution of lightning strikes around the world from January 1998 to February 2010. Image by GHCC, 2010.

All MT soundings were edited and smoothed using two different smoothing algorithms resulting in two models for each profile line (Figure 10). One model was created from a 2D inversion of both the TE and TM modes using a numerical smoothing option of the sounding

curves. The numerical smoothing option applies a fast fourier transform analysis of the soundings four components. An independent smoothed curve is then generated for each component. The second method applied to the impedance and phase curves was a D+ smoothing algorithm. The D+ algorithm examines the apparent resistivity and its corresponding phase to estimate the 1D Earth of best fit (Beamish and Travassos, 1992). The D+ smoothing algorithm is preferred as it ensures all smoothed curves generated from the sounding data are in agreement with both the phase and apparent resistivity.

All of the MT tensor data were downloaded from the Stratagem and processed using Geosystem's WinGLink software package, which utilizes the 2D inversion algorithm developed by Rodi and Mackie (2001). The flow chart presented in Figure 11 outlines the steps followed to generate the inverted 2D models of the MT data.

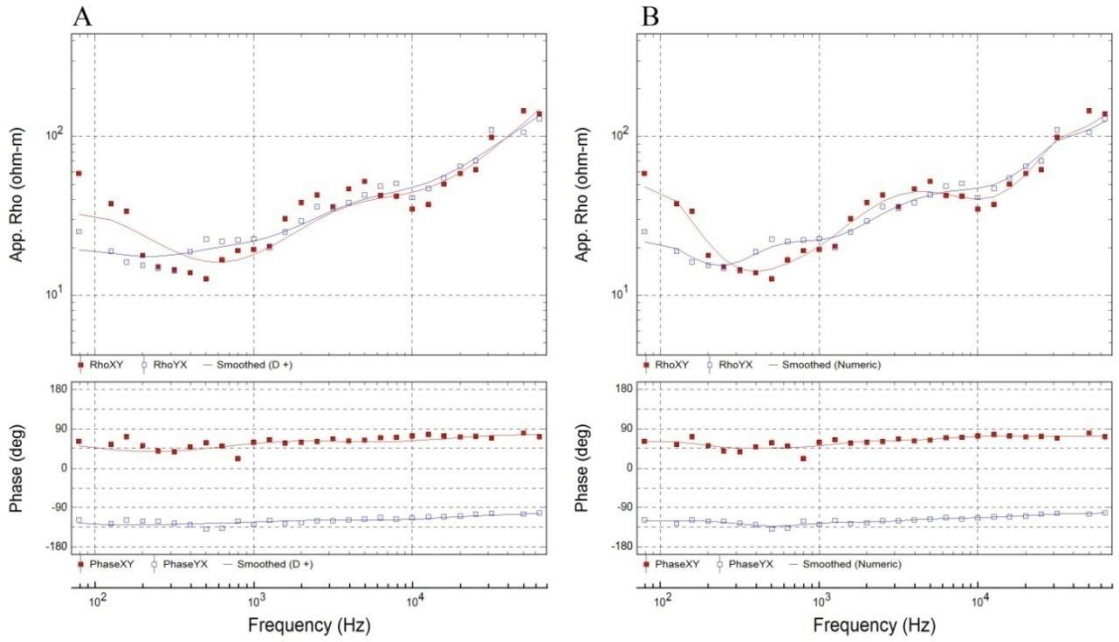

Figure 10: Side by side comparison of smoothed curves generated from the two different smoothing methods on station OS2. The smoothed curve on sounding A is generated by the D+ algorithm. The smoothed curve on sounding B is achieved through the numerical method.

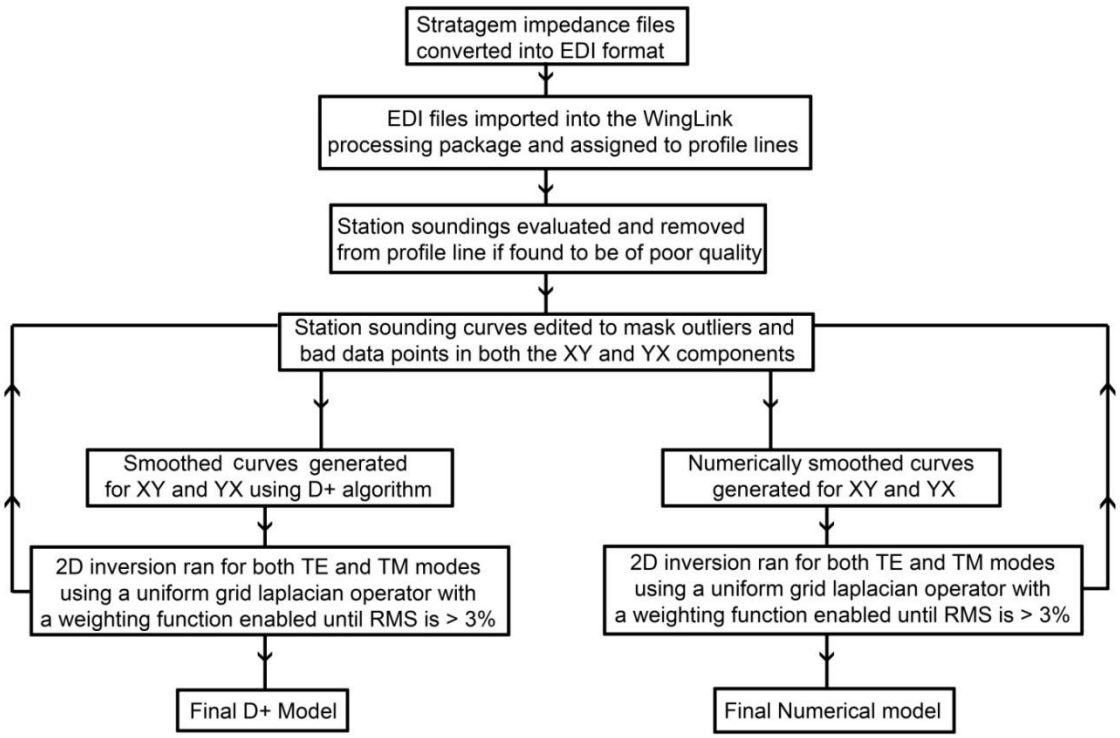

Figure 11: Data processing flow chart for the MT 2D inversion models.

CHAPTER III

RESULTS

The first sand sample taken from the center of Wadi Kobbania resulted in a specific conductance and TDS of 37.5 µS/cm and 25 mg/L. The second sample yielded a conductivity of 40.3 µS/cm and a TDS of 26.8 mg/L. The major cations measured in the samples included sodium and calcium with minor amounts of potassium and magnesium. The major anions found were chloride and bicarbonate, with minor amounts of sulfate.

Figure 12 is a 2D inversion of smooth D+ curves generated from station soundings on profile 1. A ~1200 m wide low resistivity body of < 5 Ohm-m is apparent extending northeast between the distances 2100 m and 3200 m of the profile where the southwestern end of the profile is assigned to the origin or distance zero. The deepest point of this anomaly, which extends to a depth of ~220 m, is near location 2650 m. This low resistivity zone is suggested here to correspond to the extent of loosely consolidated sedimentary rocks that fill Wadi Kobbania. Another boundary at the same location can be identified as the depth increases to ~305 m where resistivity rises above 11 Ohm-m. This resistivity boundary might be corresponding to the nonconformity separating the Precambrian crystalline rocks and the Cretaceous Nubian Sandstone formations. A low resistivity area is also apparent on the northeastern side of the profile line between distances 3500 m and 4900 m.

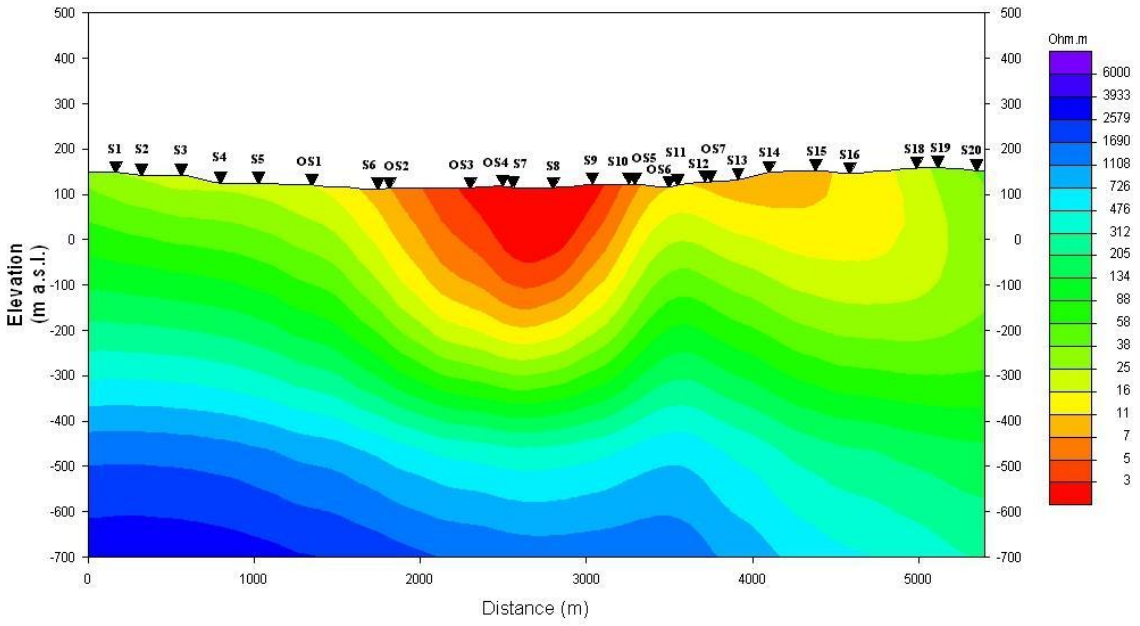

Figure 12: 2D Inversion of station soundings from Profile 1 smoothed using the D+ algorithm.

Figure 13 is a 2D inversion of numerically smoothed curves generated from station soundings on profile 1. The numerically smoothed inversion model is similar to the D+ inversion model in that the low resistivity 5 Ohm-m boundary is also imaged at ~220 m depth beneath location 2650 m. However, this model shows the low resistivity anomaly as being a broader feature encompassing a distance of ~1700 m across. This model also differs from the D+ model in that the 11 Ohm-m boundary appears to be 20 m shallower located at a depth of ~285 m. Similar to the D+ model, the numerically-smoothed model shows the eastern side of the profile between 4000 m and 4900 m as underlain by relatively low resistivity.

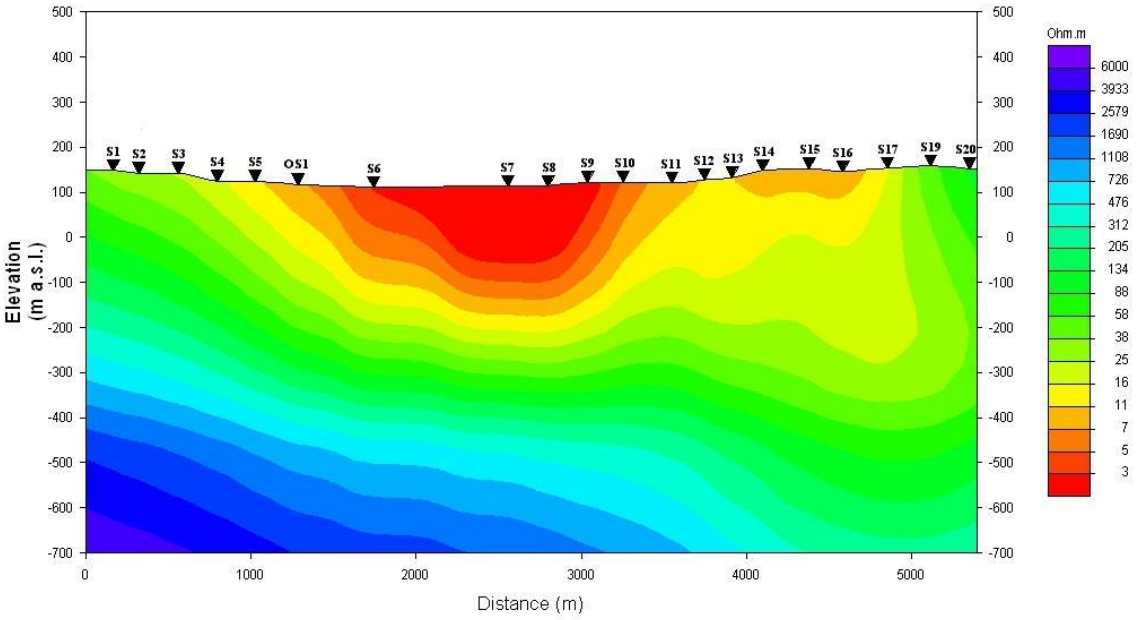

Figure 13: 2D Inversion of station soundings from Profile 1 smoothed Numerically.

Figure 14 is a 2D inversion of D+ smoothed curves generated from station soundings along profile 2. Profile 2 shows a ~1000 m wide low resistivity zone of less than 5 Ohm-m extending from distance 1600 m to 2700 m and reaching a maximum depth of ~164 m beneath the 2700 m mark. The 11 Ohm-m boundary occurs at a depth of ~440 m. On the southwestern side of the profile, near a distance of 500 m from the origin, the 11 Ohm-m boundary shallows significantly to reach a depth of only ~80 m suggesting that the Precambrian crystalline rocks are near the surface. This observation is in good agreement with seismic refractions results (Atef, 2010). A low resistivity zone of 3 Ohm-m is located on the northeastern side of the profile between distances ~4100 m and ~4750 m. There is a 900 m long gap in the profile line due to the presence of a dissected alluvial fan containing large cobbles that prevented reliable soundings from being obtained at that location.

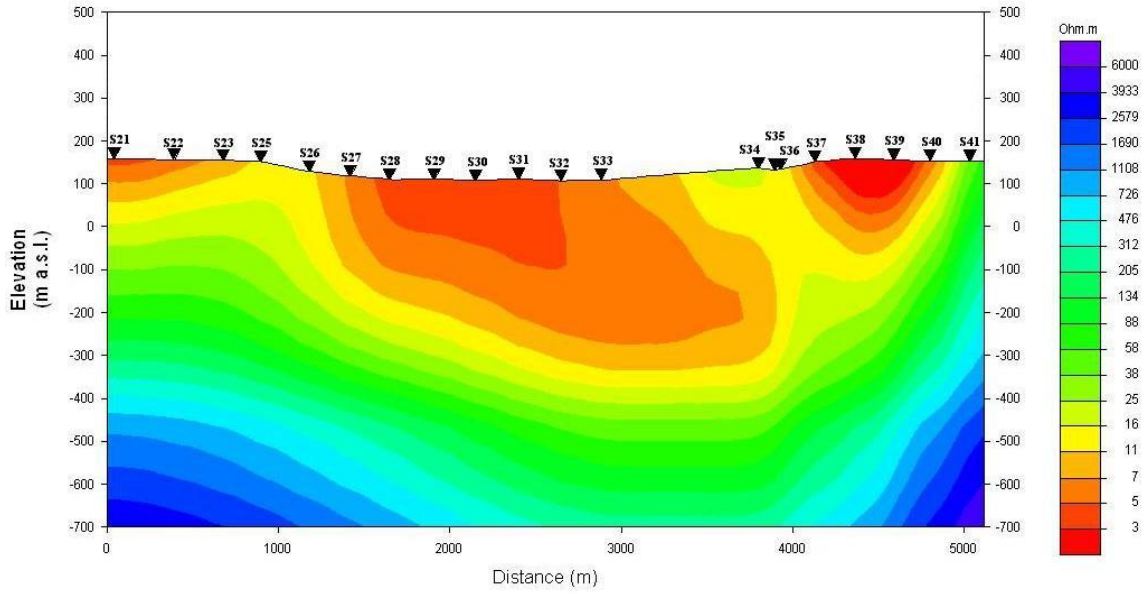

Figure 14: 2D Inversion of station soundings from Profile 2 smoothed with the D+ algorithm.

Due to the ambiguous nature of gravity data, four different gravity models have been created. To reduce the ambiguity, each model was constructed using parameters constrained from the MT model in either Figure 12 or Figure 13. Subsequently, for each of the constraints provided by the two different smoothed MT models, two independent gravity models were created to represent the Wadi Kobbania as either a graben or as an incised valley. All density values assigned to the different rock units were from the values calculated from rock samples obtained from the study area.

Figure 15 is a gravity model created from using constraints provided by the D+ model in Figure 12. Additional constraint applied to this model was using a maximum thickness of 160 m for the Nubian Sandstone formations as suggested by the surface exposures of these formations around the Aswan area. The model shows a 2200 m wide section of low density (2.1 g/cm^3) extending between 2100 m and 4300 m with a maximum depth of ~170 m beneath location 3210 m. This part of the gravity model, labeled as "Post-Cretaceous Fill", accounts for the presence of

loosely-consolidated sandstone and conglomerate that seem to fill Wadi Kobbania. This unit sits on top of the Wadi Kobbania Nubian Sandstone formations which progressively deepen toward the center of the wadi and are modeled with an average density of 2.4 g/cm^3. The deepest part of the Nubian Sandstone formation is present in the middle of the graben at location 3210 m with a thickness of ~140 m. In this location, the Precambrian crystalline rocks, which are modeled with an average density of 2.62 g/cm^3, are predicted to be encountered at depth of ~310 m. At the southwestern and northeastern flanks of the wadi the Precambrian crystalline rocks are predicted to be encountered at a depth of only ~80 m. In this model, a 24 m thick layer of 2.0 g/cm^3 is introduced to account for an exposed, but heavily disturbed Nubian Sandstone unit resulting from bulldozing during road construction as well as the presence of large sand dunes. This unit extends in the southwestern side of Wadi Kobbania between locations 0 m and 750 m.

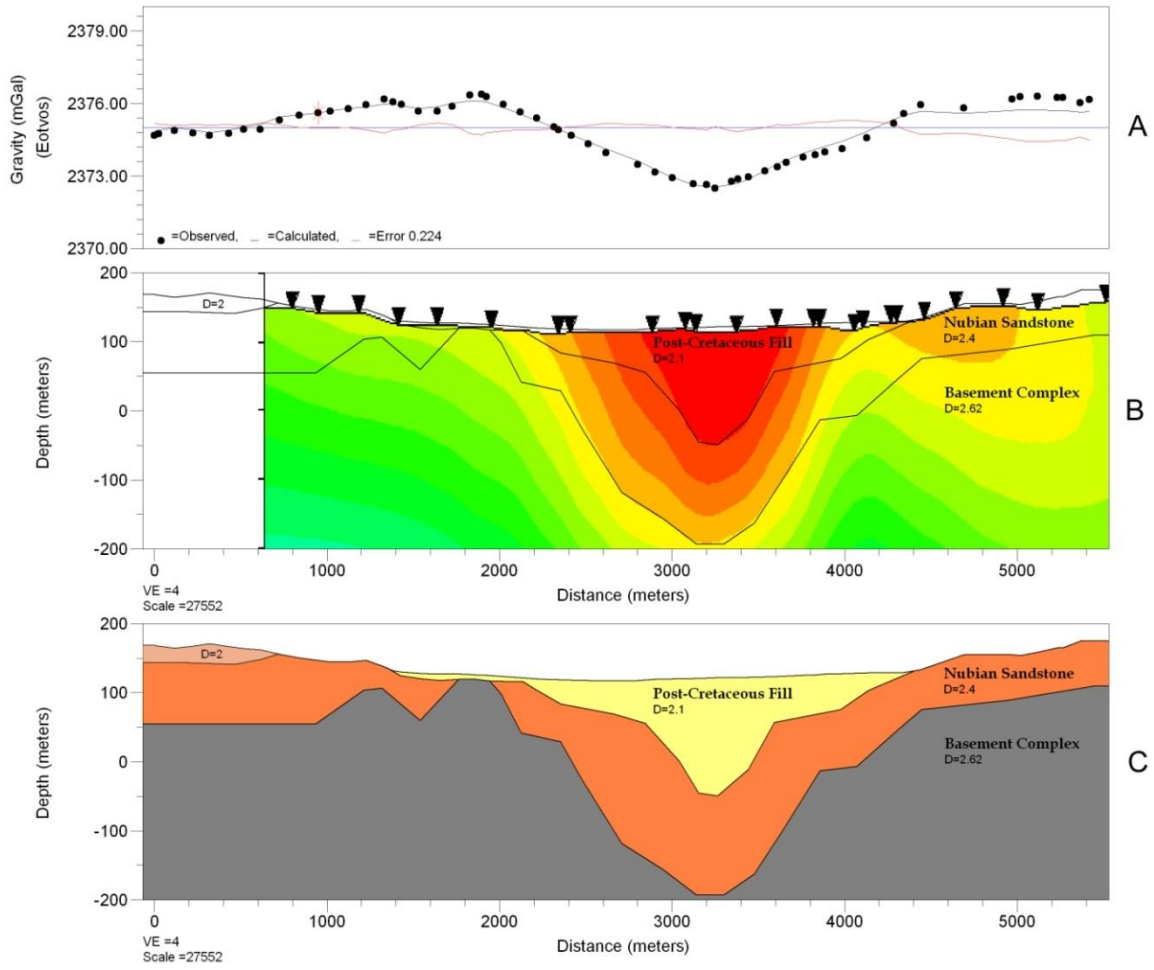

Figure 15: Graben model of Profile 1 structured around the D+ smoothed MT model. A) Black dots represent the observed gravity curve corrected to base station. Black line represents the calculated gravity curve generated from the model. The red line is the error value and represents how closely the observed and calculated curves fit together. B) Gravity model overlying the 2D inverted D+ model. C) Final gravity model, Nubian group was assigned a density of 2.4 g/cm^3, basement density=2.62 g/cm^3, disturbed Nubian density =2 g/cm^3, and post-Cretaceous fill density=2.1 g/cm^3

Figure 16 is a gravity model created with the guidance of the numerically smoothed MT model in Figure 13. The 11 Ohm-m boundary is selected as depicting the unconformity between the Precambrian crystalline rocks and the Cretaceous sandstone formations similar to what has been adopted for the model in Figure 15. This model is similar to that in Figure 15 at the northeastern and southwestern margins of Wadi Kobbania. However, this model differs slightly

from the one in Figure 15 in estimating the thickness of the post-Cretaceous fill. In this model, maximum thickness of the post-Cretaceous fill is estimated to be ~150 m below location 3210 m. Also, at this location the thickness of the Nubian Sandstone formation is estimated to be ~10 m thicker than that of the model in Figure 15 reaching a thickness of 150 m and the depth to the Precambrian crystalline rocks is shown to be around the 300 m. In general, the models in both Figure 15 and Figure 16 are in good agreement with each other. The D+ smoothed MT model shown in Figure 15 appears to correlate better with the depth of boundaries between different geological units estimated in the gravity model.

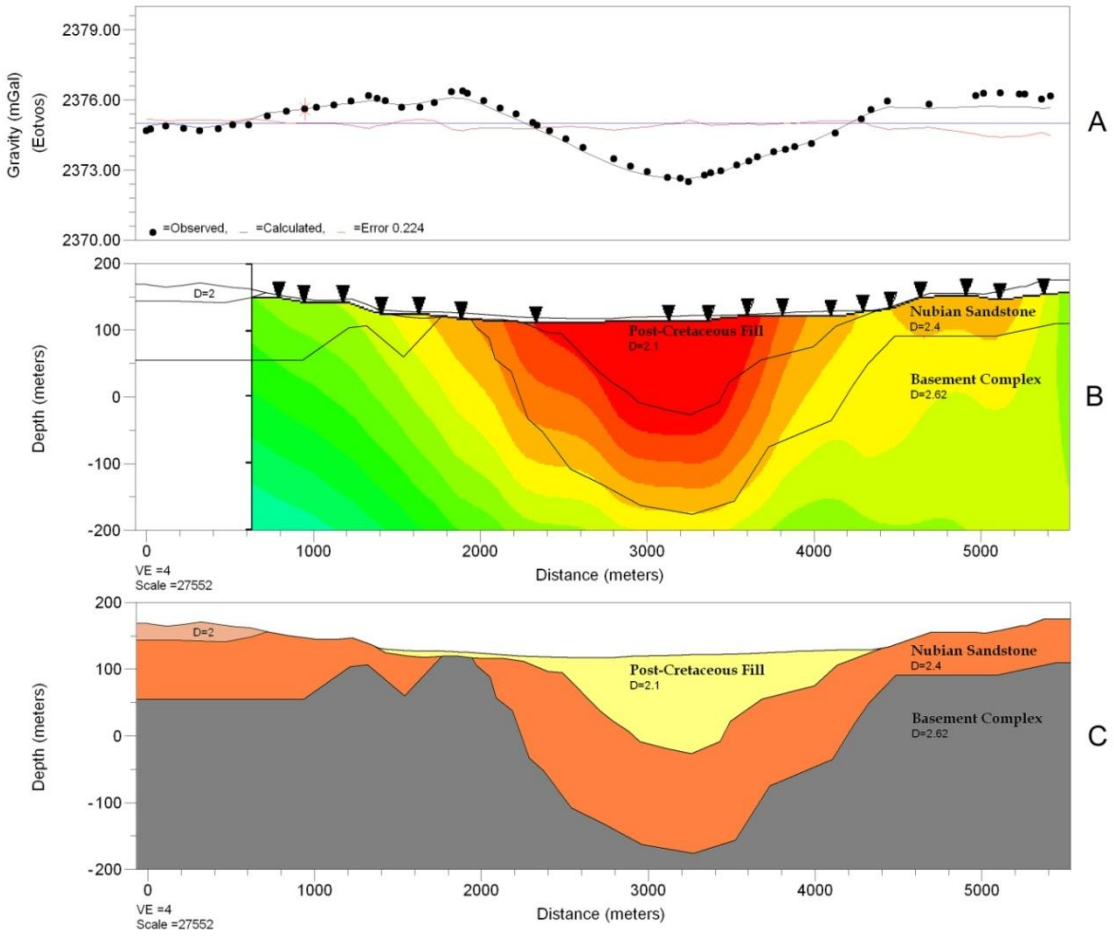

Figure 16: Graben model of Profile 1 structured around the numerically smoothed MT model. A) Black dots represent the observed gravity curve corrected to base station. Black line represents the calculated gravity curve generated from the model. The red line is the error value and represents how closely the observed and calculated curves fit together. B) Gravity model overlying the 2D inverted numerical model. C) Final gravity model, Nubian group was assigned a density of 2.4 g/cm^3, basement density=2.62 g/cm^3, disturbed Nubian density =2 g/cm^3, and post-Cretaceous fill density =2.1 g/cm^3

It should be emphasized that the graben models only reflect the predicted depth distribution of the Precambrian crystalline rocks, the Nubian Sandstone formations, and the post-Cretaceous fill based upon their estimated density values. The polygons of each unit have been smoothed and do not reflect the structural complexity of the graben. Figure 17 is a conceptual model showing normal faulting required to form the graben structures shown in Figure 15C and Figure 16C.

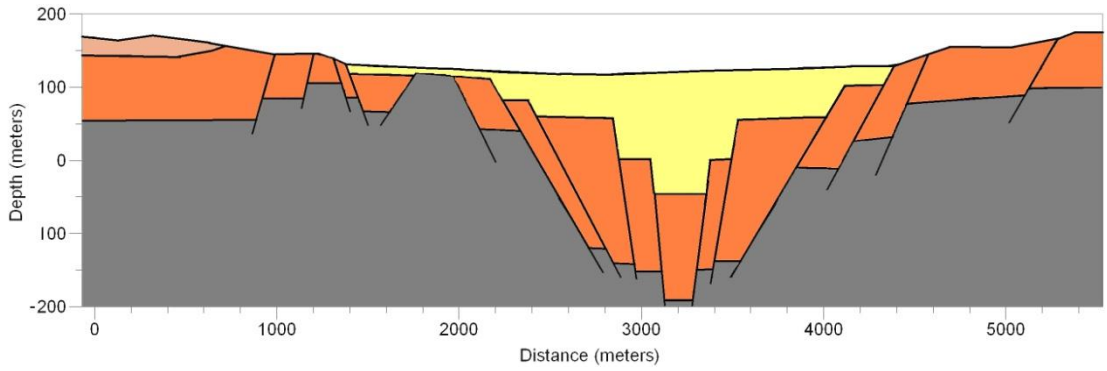

Figure 17: Conceptual model illustrating the Wadi Kobbania as a graben filled with post-Cretaceous sedimentary rocks.

The gravity data across the Wadi Kobbania can equally be modeled as resulting from a valley that has incised through the Cretaceous sandstone formations and the Precambrian crystalline rocks and later was filled with post-Cretaceous sedimentary rocks. Figure 18 is a gravity model created using the D+ MT model shown in Figure 12 as a reference. This model was created in order to represent the gravity and MT data as manifesting an incised valley. This model predicts that the Cretaceous sandstone formations are only present at the northeastern and southwestern boundaries of Wadi Kobbania with an average thickness of ~80 m keeping the depth to the top of the Precambrian crystalline basement consistent with the two graben models in Figure 15 and Figure 16. The model shows a 2300 m wide valley extending between locations 2100 m and 4400 m and reaching a maximum depth of ~220 m. This model predicts complete erosion of the Nubian Sandstone formations during the valley incision. At location 3210 m (which corresponds to the deepest part of the valley) the top of the Precambrian crystalline rocks is predicted to be at ~220 m depth corresponding to the 5 Ohm-m resistivity boundary on the MT model shown in Figure 12. This gravity model does not account for the two gravity highs at the 1300 m and 1850 m mark.

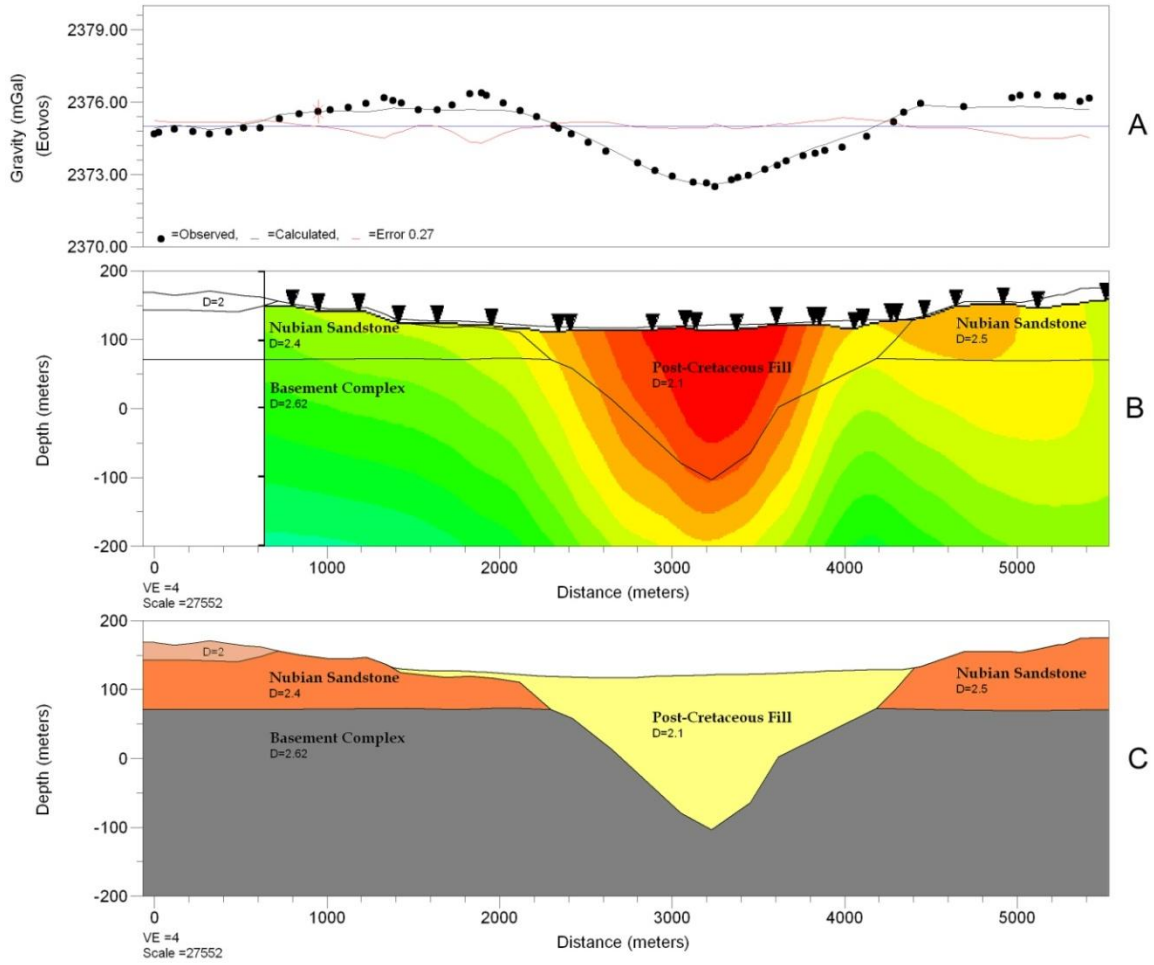

Figure 18: Incision model of Profile 1 structured around the D+ smoothed MT model. A) Black dots represent the observed gravity curve corrected to base station. Black line represents the calculated gravity curve generated from the model. The red line is the error value and represents how closely the observed and calculated curves fit together. B) Gravity model overlying the 2D inverted D+ model. C) Final gravity model, Nubian group was assigned a density of 2.4 g/cm^3 to the west and a slightly denser 2.5 g/cm^3 to the east, basement density=2.62 g/cm^3, disturbed Nubian density =2.0 g/cm^3, and post-Cretaceous fill density =2.1 g/cm^3

Figure 19 is a gravity model created by using the numerically smoothed MT model shown in Figure 13. The model is identical to the model of Figure 18, except for a slight discrepancy in the shape of the valley resulting in locating the depth to the Precambrian crystalline rocks at ~200 m. The gravity highs at 1300 m and 1850 m are not accounted for by this model.

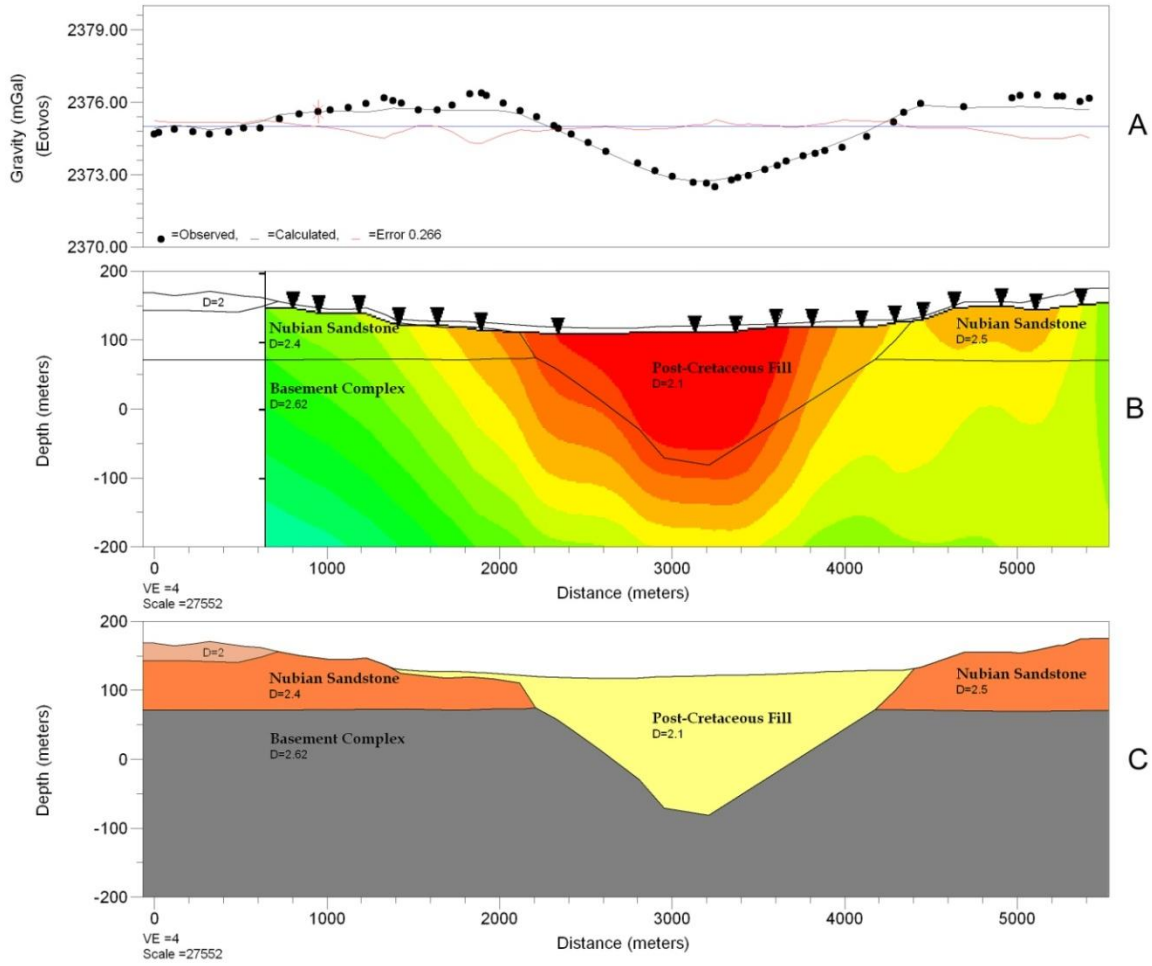

Figure 19: Incision model of Profile 1 structured around the numerically smoothed MT model. A) Black dots represent the observed gravity curve corrected to base station. Black line represents the calculated gravity curve generated from the model. The red line is the error value and represents how closely the observed and calculated curves fit together. B) Gravity model overlying the 2D inverted D+ model. C) Final gravity model, Nubian group was assigned a density of 2.4 g/cm^3 to the west and a slightly denser 2.5 g/cm^3 to the east, basement density=2.62 g/cm^3, disturbed Nubian density =2.0 g/cm^3, and post-Cretaceous fill density =2.1 g/cm^3

CHAPTER IV

DISCUSSION

Two independent geophysical data sets (MT and gravity) were used to image the subsurface architecture of Wadi Kobbania in order to determine the nature of the geomorphological and structural features influence on the course of paleodrainage of Wadi Abu Subeira – Wadi Kobbania. All MT models indicate the presence of a large conductive body extending ~200 m below Wadi Kobbania. Low resistivity areas inferred in the northeastern part of MT Profiles 1 and 2, (Figure 12-Figure 14), are likely due to interference from a small NE-SW channel in close proximity to the profile lines.

The leaching experiments on the sand samples collected from the wadi suggest the conductive feature is likely due to the presence of salt, primarily halite, possibly indicating a saline environment if an aquifer is present. The observed gravity curve across the wadi shows a gravity low indicating the presence of less dense geological unit(s), possibly the Cretaceous sandstone formations and/or post-Cretaceous sedimentary rocks on top of denser Precambrian crystalline rocks located at ~200 m depth under Wadi Kobbania. The gravity and MT models indicate that Wadi Kobbania is either incised much deeper than what was previously suggested or that it is actually a graben that has been filled with post-Cretaceous clastic sedimentary rocks. Below is a discussion aimed at making the case for favoring the graben model.

4.1 Why the Incision Model cannot be Supported?

The incision models shown in Figure 18 and Figure 19 suggest a ~2300 m wide incised valley with a depth ranging between ~200 m and ~220 m; a depth reaching ~80 to ~110 m below present day modern sea level (MSL). These models clearly show that the Wadi Kobbania is a much deeper geological feature than the 40 m incision depth estimated by Wendorf and Schild (1976). Such deep incision requires it to be accompanied by a comparable regional uplift or sea level drop. There is no evidence that post-Cretaceous regional uplifting has affected the region other than the Oligocene rift-flank uplift associated with the opening of the Red Sea exposing the Precambrian crystalline rocks in the Eastern Desert of Egypt. This uplift was restricted to the Red Sea Hills east of the Nile and did not extend to the west as evidenced by the present day topography where the vastly expanding Galabala plain only rises ~150 m above MSL. However, it can be argued that such a deep incision of Wadi Kobbania may have been triggered by the sharp drop in base level during the Messinian Salinity Crisis when the Mediterranean Sea desiccated completely because the basins water circulation was cut off from the Atlantic Ocean. The depth a river will incise is ultimately controlled by base level, regardless of the volume of water it transports. Base-level change is affected primarily by tectonics and changes in eustatic sea level and are a major influence upon rivers because of changes to the river systems potential energy, as well as its sediment supply (Keller and Pinter, 1996). Typically, a drop in sea level results in active down-cutting or incision. However, rivers can also accommodate decreasing base level by changing other variables such as sinuosity or channel pattern with little or no incision, but rapid drop in base level tends to favor incision (Keller and Pinter, 1996). The complete desiccation of the Mediterranean sea during the late Miocene resulted in a rapid drop in base level by thousands of meters below MSL (Hsu et al., 1973). This resulted in the cutting of the Eonile canyon, which is 100's of meters deep, into older marine sedimentary rocks in order to establish equilibrium with the rapid lowering of base level. This canyon was subsequently filled

with sediments during the early Pliocene when the Mediterranean Sea reestablished its connection to the Atlantic Ocean (Hsu et al., 1973; Keller and Pinter, 1996). During this event the Eonile Canyon at Aswan incised a gorge 200 m below sea level, 1250 km (4 times longer than the Grand Canyon) from the shorelines of the Mediterranean sea (Hsu et al., 1973). The Eonile Canyon stretches all the way from the Mediterranean sea beneath Cairo with a uniform width of 10-20 km (Hsu et al., 1973; Said, 1981). The Eonile canyon was discovered in 1970 by the Russian scientist I.S. Chumakov during the construction of the Aswan High Dam. Boreholes drilled along the sides of the Nile encountered the Nubian Sandstone formations at ~30 m depth. When drilling in the center of the Nile River the Nubian Sandstone formations were unexpectedly absent and only fluvial sediments were encountered before encountering the Precambrian crystalline rocks at 275 m depth (Said, 1981). Hence, the ~200 m depth of Wadi Kobbania could have been the result of a rapid incision of a SE-flowing river draining into the Eonile canyon which provided a local lower base-level. Additionally, it can be argued that the conductive signature of the sediments filling the wadi reflects an estuarine depositional environment resulting in the deposition of evaporates as a result of back-flooding of Wadi Kobbania during the Gulf phase, which occurred 5.4 to 3.3 Ma after the resumption of water circulation between the Mediterranean sea with the Atlantic Ocean (Figure 3; Said, 1993). A major weakness of this model is the required large discharge sourced from the limestone of the Sin el Kaddab Plateau to the west. This prediction of the model is not supported by geological observations, which indicate that at least the upper part of Wadi Kobbania is filled with clastic sediments sourced from the Precambrian crystalline rocks of the Red Sea Hills to the east and that paleo-current data clearly points to these sediments being deposited in a drainage system that was flowing to the northwest. In addition, regional and eustatic sea level from the Cretaceous through the Messinian Salinity Crisis during the late Miocene was marked by a regression. However, sea level in the region at this time was still higher than present sea levels and would not have facilitated a ~200 m deep incision in Wadi Kobbania, especially one that would reach ~80-100 m below MSL

(Figure 20). Hence, the absence of any limestone clasts in the Wadi Kobbania and the lack of any other major changes in base level rules out the possibility that the ~200 m depth of Wadi Kobbania was achieved through river incision.

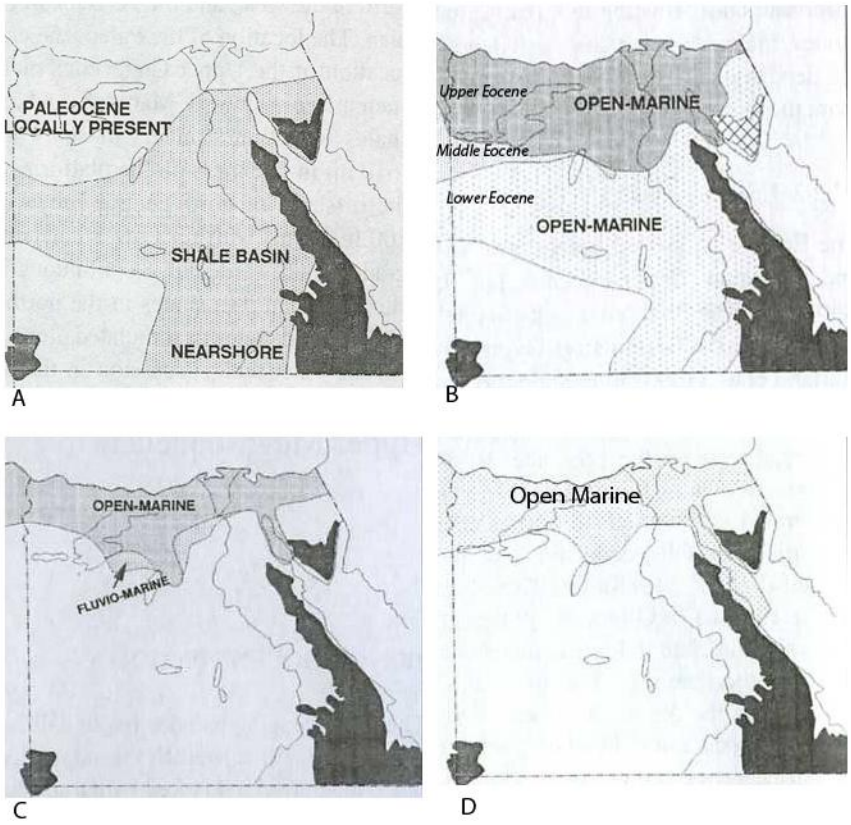

Figure 20: Paleogeographic maps showing the depositional environments during the Paleocene, Eocene, Oligocene, and Miocene which can be used to infer the relative sea level at the time. A.) Paleocene paleogeographic map B.) Eocene paleogeographic map C.) Oligocene paleographic map D.) Miocene paleogeographic map. Compiled from (Tawardros, 2001).

4.2 Support for a Graben Model for Wadi Kobbania

Estimates predict between 25 to 75% of all continental drainage in unglaciated regions has been either tectonically influenced or controlled with some rivers maintaining the same drainage course for 1/16th of the Earth's entire history due to the presence of structural features (Melton, 1959; Schumm et al., 2000). Extensional deformation of the crust forms a characteristic

topography of upthrown and downthrown blocks, i.e. horsts and graben structures. Drainage patterns readily follow the trend of these extensional structures where through-going rivers exploit the low topography presented by grabens (Schumm et al., 2000). Widespread NW-trending normal faults were formed in northeast Africa in the Late Oligocene through the early Miocene when the Arabian plate began to move to the northeast away from the stationary African plate (Makris et al., 1991; Morgan, 1990; Tawardros, 2001). The Kobbania graben is likely an extensional feature resulting from this movement. The presence of this graben can effectively explain the abrupt NW deflection and depths achieved in the Wadi Abu Suberia-Wadi Kobbania paleodrainage as it was approached and subsequently captured by the Wadi Kobbania graben.

The graben models shown in Figure 15 and Figure 16 suggest a post-Cretaceous fill with a depth of ~150 to ~170 m from the top of the Nubian Sandstone formations. These depths would result in the fill reaching 25-50 m below present MSL. This depth represents an accurate estimation of the depth of negative topography existing shortly after the Wadi Kobbania graben. This topographic low would quickly become filled by aggraded sediments eroded and subsequently transported from the Precambrian crystalline rocks of the uplifted Red Sea Hills as well as the surrounding Nubian Sandstone formations as the newly-formed drainage system moved toward achieving topographic equilibrium.

Several factors indicate structural activity in the area of Wadi Kobbania. Observation of the outcropping Umm Barmil Formation, comprising the plateaus to the northeast and southwest of the wadi, contain numerous fractures indicating fault movement (Figure 21). Remotely-sensed lineaments (Figure 2), interpreted by Lansbery (2010), also show the presence of NW trending structures in the area of the Wadi Kobbania. The gravity profile shows a gravity high feature of ~1 mGal between locations 1000 m and 2100 m. Outcrops displaying the unconformity between the Cretaceous aged Nubian Sandstone and the Precambrian crystalline basement suggest the underlying crystalline rocks are usually untilted and tabular in form. Hence, this gravity feature

cannot be modeled in terms of three unfaulted layers constituting post-Cretaceous fill underlain by the Cretaceous sandstone formations which in turn are underlain by Precambrian crystalline rocks.

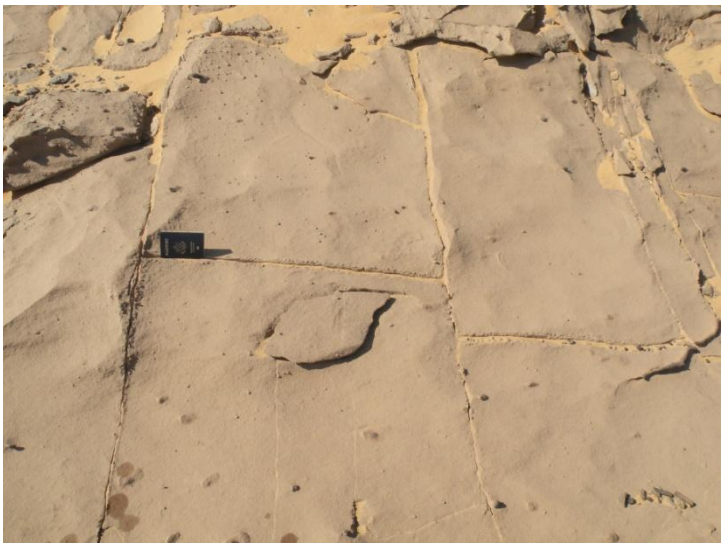

Figure 21: Exposed Umm Barmil Formation on the northeastern plateau of Wadi Kobbania.

Rather, this gravity high feature can be modeled with the post-Cretaceous fill sitting directly on top of the Precambrian crystalline rocks (Figure 15-Figure 17). This structure is likely due to the superposition of at least two discrete phases of extension. The first phase cut the Precambrian crystalline rocks and the overlying Cretaceous sandstone formations forming horsts and grabens with parts of the Precambrian crystalline rocks preserved on horst structures at structurally-high levels. Subsequent erosion removed the Nubian Sandstone formations from the top of the horst structures but these formations were preserved within the grabens. During the second phase of extension, the graben fill was redeposited on top of the preserved Nubian Sandstone formations as well as the uplifted Precambrian crystalline rocks. This interpretation is in good agreement with results of seismic refraction studies by Atef 2010 (unpublished data). The seismic refraction model (Figure 22) strongly correlates with the graben models for Wadi Kobbania derived from gravity and MT data. The seismic model also shows an uplifted block of Precambrian crystalline

rocks on the southwestern side of Wadi Kobbania in which the post-Cretaceous fill directly overlies the Precambrian crystalline rocks.

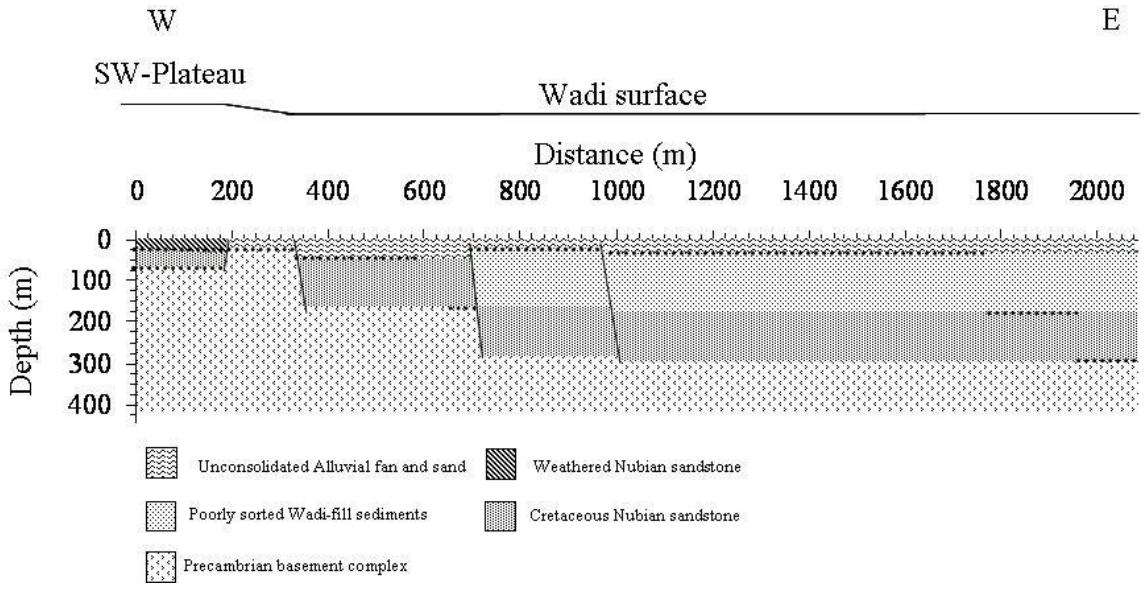

Figure 22: Subsurface model of the western half of Wadi Kobbania from seismic refraction data, gathered and interpreted by Atef (2010).

Fission track results by Omar and Steckler (1995) have shown that the opening of the Red Sea occurred simultaneously along its entire length with the early stages of rifting characterized by two pulses of uplift at ~34 Ma and 21-25 Ma. Considering these regional tectonic constraints, it can be suggested that the Wadi Kobbania graben was formed during these two extensional tectonic pulses and the post-Cretaceous fill was probably deposited during the early to mid-Miocene before the development of the Eonile canyon, which would have resulted in isolating the graben from sediment supplied from the Red Sea Hills around 6 Ma.

Similar NW trending features are seen in Shuttle Imaging Radar C-band (SIR-C) and X-band Synthetic Aperture Radar (X-SAR) images as far northwest as ~400 km along-strike of the Kobbania graben close to the city of Assuit (Figure 23). These interpreted graben structures (Figure 23C) are strikingly similar in their trend and width (3-4 km) to that of the Wadi Kobbania

graben. These similarities are intriguing and suggest that the Wadi Kobbania is the southeastern extension of the Assiut grabens.

The 2D models (Figure 15-Figure 17) of the Kobbania graben predict a total vertical displacement in excess of ~250 m. The lack of other known NW trending grabens in the Aswan area, as well as the narrow width and relatively large displacement of the Kobbania graben, suggests a strongly-focused strain localization within NW-trending normal faults in southern Egypt. Strain localization occurs when strain felt on the majority of the rock structure unloads, localizing into narrow bands of intense straining resulting in >80% of the total strain being relieved by a small number of large faults (Cowie et al., 2007; Jirásek, 2002). It would be of interest to compare fault displacement of the Kobbania graben with fault displacement accommodated within the grabens around the city of Assiut. It is likely that the Assiut structures will exhibit a smaller displacement than what is observed in the Kobbania graben, as the extension seems to have been distributed across the numerous grabens of the area.

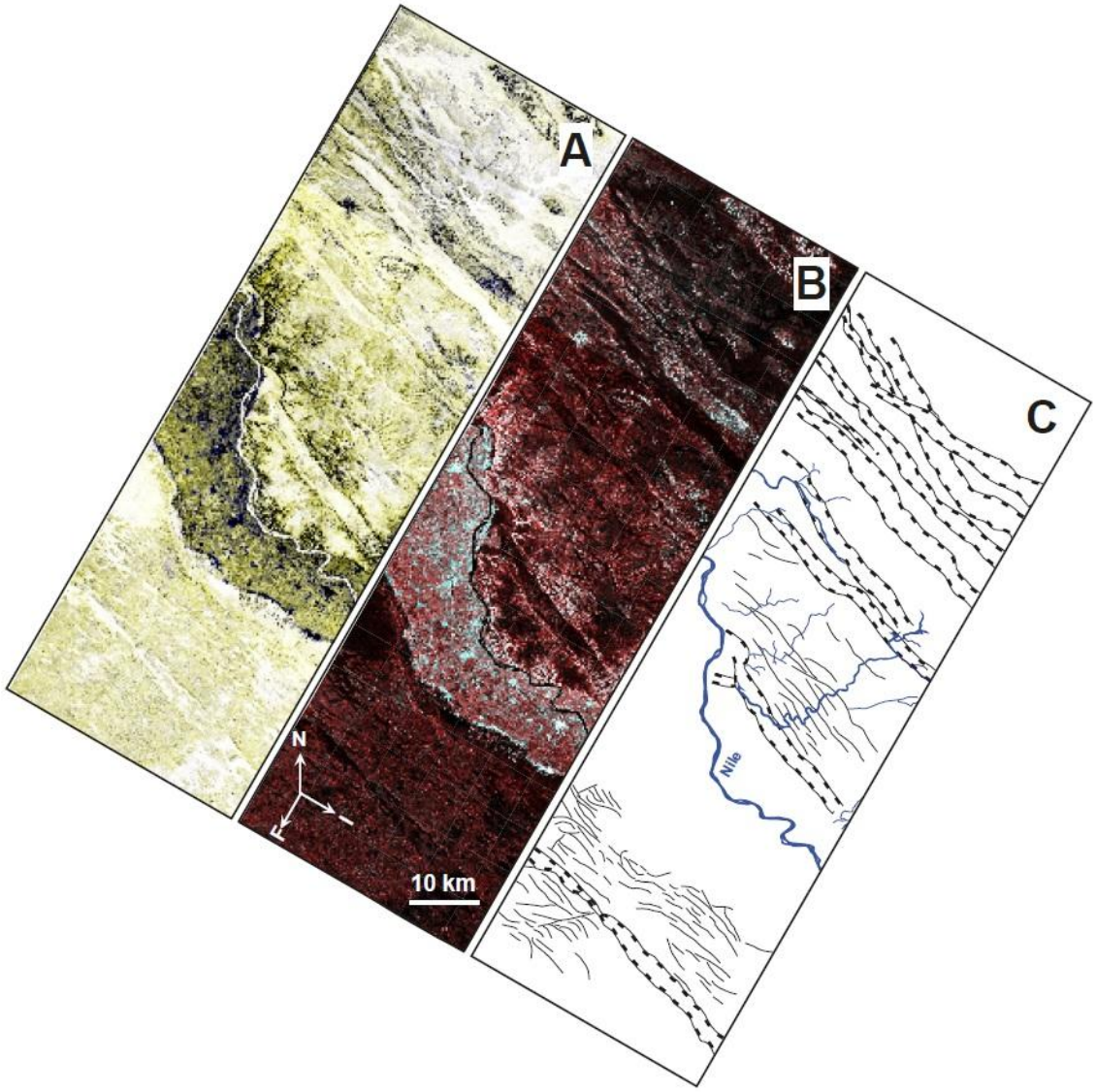

Figure 23: Narrow NW trending graben structures around the city of Assiut. A) 1/Lhh-1/Lhv-1/Chv SIR-C/X-SAR image. B) Lhh-Lhv-Chv SIR-C/X-SAR image. C) Structural interpretation of the radar image in A. Lines with solid squares represent normal faults with the solid squares showing the throw direction of the hanging wall. Lines with no solid squares represent surface projection of fault heaves. The abbreviations in the arrow are: N = North, I = Radar illumination direction and F = Shuttle flight direction.

CHAPTER V

CONCLUSION AND RECOMMENDATIONS FOR FUTURE WORK

Many western flowing Oligocene rivers in Egypt were sourced from the uplifted Red Sea Hills in the Eastern Desert. The Wadi Kobbania-Wadi Abu Subeira paleodrainage was one of these western flowing rivers which drained southern Egypt during the Tortonian prior to onset of the Eonile canyon ~6 Ma ago and possibly the mid-Pleistocene. Models generated from MT and gravity data show the structure of Wadi Kobbania extends much deeper into the subsurface than previously anticipated. River incision to the depths observed in the Wadi Kobbania could have occured during the Messinian Salinity Crisis, but the absence of limestone clasts filling the Wadi Kobbania does not support this argument. Regional tectonics and the local structures developed in Aswan clearly influenced the drainage systems of the Pre-Eonile period, as the geophysical models and geologic history of the area support the hypothesis that Wadi Kobbania is a structural graben bounded by NW trending faults formed from extensional tectonics during the Oligocene. The presence of this graben explains the sudden NW deflection seen in the Wadi Kobbania paleodrainage. In order to place further constraints on the extent and size of the graben, several more profiles should be acquired across the wadi. Additional profiles across some of the NW trending structures observed from the SIR-C and X-SAR images of the Eastern and Western Desert near the city of Assiut (Figure 23) would also be of interest. Data obtained from these profiles might indicate that the Wadi Kobbania graben is a southeastern extension of these structures, which would have formed contemporaneously. However, it is recommended to use the gravity and magnetic methods instead of MT, for these additional profiles, due to the weak

MT signal in northeastern Africa and contact issues with electrodes.

The depth of the Kobbania graben extends well beneath the current base of the Nile River and provides an optimistic location to drill groundwater wells. Strain localization on faults within the Precambrian crystalline rocks is suggested by the narrow width of the graben, amount of subsidence observed from cross-sectional models, and lack of other known NW trending grabens in the area. Analyses of sedimentary rocks to be recovered from wells drilled within the graben would be of great interest. If these sedimentary rocks are determined to be sourced from the Red Sea Hills, it will provide stronger evidence that the Kobbania graben captured the drainage system of Wadi Abu Subeira before being superimposed by the Eonile canyon.

REFERENCES

Abdelsalam, M.G., Robinson, C., El-Baz, F., and Stern, R.J., 2000, Applications of Orbital Imaging Radar for Geologic Studies in Arid Regions: The Saharan Testimony: Photogrammetric Engineering and Remote Sensing v. 66, p. 717-726.

Atef, A., 2010, Seismic refraction investigation of Wadi Kobbania: Rolla, Missouri S&T

Attia, M.I., 1955, Topography, geology and iron-ore deposits of the district east of Aswan: Cairo, Egyptian Geological Survey, 262 p.

Beamish, D., and Travassos, J.M., 1992, The use of the D+ solution in magnetotelluric interpretation: Journal of Applied Geophysics, v. 29, p. 1-19.

Bedrosian, P., 2007, MT+, Integrating Magnetotellurics to Determine Earth Structure, Physical State, and Processes: Surveys in Geophysics, v. 28, p. 121-167.

Butzer, K.W., and Hansen, C.L., 1968, Desert and river in Nubia; geomorphology and prehistoric environments at the Aswan reservoir: Madison, University of Wisconsin Press, p. 562.

Cagniard, L., 1953, Basic theory of the magneto-telluric method of geophysical prospecting: Geophysics, v. 18, p. 605-635.

Conoco, 1987, Geological Map of Egypt 1:500,000, *in* Klitzsch, E., List, F.K., and Pöhlman, G., eds.: Cairo, The Egyptian General Petroleum Corporation.

Cowie, P.A., Roberts, G.P., and Mortimer, E., 2007, Strain localization within fault arrays over timescales of 10^0–10^7 years, *in* Handy, M.R., Hirth, G., and Hovius, N., eds., Tectonic Faults: Agents of Change on a Dynamic Earth, Volume Dahlem Workshop Report 95: Cambridge, p. 47-77.

EGSMA, 1981, Geologic map of Egypt, Egyptian Geological Survey and Mining Authority.

El Bastawesy, M., Faid, A., and Gammal, E.S.E., 2010, The Quaternary development of tributary channels to the Nile River at Kom Ombo area, Eastern Desert of Egypt, and their implication for groundwater resources: Hydrological Processes, v. 24, p. 1856-1865.

El Naggar, Z.R., 1970, On a proposed lithostratigraphic subdivision for the Late Cretaceous-Early Paleogene succession in the Nile Valley, Egypt, 7th Arab Petroleum Congress, Volume 64: Kuwait, p. 1-50 B-3.

Gani, N.D.S., Gani, M.R., and Abdelsalam, M.G., 2007, Blue Nile incision on the Ethiopian Plateau: Pulsed plateau growth, Pliocene uplift, and hominin evolution: GSA Today, v. 17, p. 4-11.

GHCC, 2010, Global Lightning Image, NASA/MSFC.

Ghoneim, E., Robinson, C., and El-Baz, F., 2007, Radar topography data reveal drainage relics in the eastern Sahara: International Journal of Remote Sensing, v. 28, p. 1759 - 1772.

Gindy, A.R., and Tamish, M.M., 1998, Petrogenetic revision of the basement rocks in the environs of Aswan, southern Egypt: Egypt Journal of Geology, v. 42, p. 1-14.

Goudie, A.S., 2005, The drainage of Africa since the Cretaceous: Geomorphology, v. 67, p. 437-456.

Harris, N.B.W., and Gass, I.G., 1981, Significance of contrasting magmatism in North East Africa and Saudi Arabia: Nature, v. 289, p. 394-396.

Hendriks, F., Kallenbach, H., and Philobbos, E.R., 1990, Cretaceous to early tertiary continental and marginal marine sedimentary environments of southeastern Egypt: Journal of African Earth Sciences, v. 10, p. 229-241.

Hinz, E.A., Stern, R.J., Thurmond, A.K., Abdelsalam, M.G., and Abdeen, M.M., 2003, When did the Nile Begin?: Remote Sensing Analysis of Paleo-drainages Near Kom Ombo, Upper Egypt: Eos Transactions, Fall Meeting Supplement, Abstract, v. 84.

Hsu, K.J., Ryan, W.B.F., and Cita, M.B., 1973, Late Miocene Desiccation of the Mediterranean: Nature, v. 242, p. 240-244.

Issawi, B., 1969, The geology of Kurkur-Dungle area: Cairo, General Egyptian organization for Geological Research and Mining, 102 p.

Issawi, B., and McCauley, J.F., 1992, The Cenozoic Rivers of Egypt; the Nile problem, *in* Friedman, R., and Adams, B., eds., The Followers of Horus: Oxford, Oxford Monograph, p. 121-138.

Jirásek, M., 2002, Objective modeling of strain localization: Revue française de génie civil, v. 6, p. 1119-1132.

Jones, A.G., 1993, Electromagnetic images of modern and ancient subduction zones: Tectonophysics, v. 219, p. 29-45.

Keller, E.A., and Pinter, N., 1996, Active tectonics : earthquakes, uplift, and landscape: Upper Saddle River, NJ, Prentice Hall, p. 338 p.

Kerdany, M.T., and Cherif, O.H., 1990, Mesozoic, *in* Said, R., ed., The Geology of Egypt: Rotterdam/Brookfield, Balkema, p. 407-438.

Klitzsch, E.H., and Squyres, C.H., 1990, Paleozoic and Mesozoic Geological History of Northeastern Africa Based Upon New Interpretation of Nubian Strata: AAPG Bulletin, v. 74, p. 1203-1211.

Krijgsman, W., Hilgen, F.J., Raffi, I., Sierro, F.J., and Wilson, D.S., 1999, Chronology, causes and progression of the Messinian salinity crisis: Nature, v. 400, p. 652-655.

Lansberry, L., 2010, Structural controls of the Egyptian Nile River in the area between Aswan and Kom Ombo: Rolla, Missouri S&T.

Makris, J., Henke, C.H., Egloff, F., and Akamaluk, T., 1991, The gravity field of the Red Sea and East Africa: Tectonophysics, v. 198, p. 369-381.

McCauley, J.F., Breed, C.S., Schaber, G.G., McHugh, W.P., Issawi, B., Haynes, C.V., Grolier, M.J., and El Kilani, A., 1986, Paleodrainages of the Eastern Sahara—the radar rivers revisited. SIR A/B implications for a mid-Tertiary trans-African drainage system: IEEE Transactions on Geosciences and Remote Sensing, v. GE-24, p. 624-648.

McCauley, J.F., Schaber, G.G., Breed, C.S., Grolier, M.J., Haynes, C.V., Issawi, B., Elachi, C., and Blom, R., 1982, Subsurface Valleys and Geoarcheology of the Eastern Sahara Revealed by Shuttle Radar: Science, v. 218, p. 1004-1020.

Melton, F.A., 1959, Aerial Photographs and Structural Geomorphology: The Journal of Geology, v. 67, p. 351-370.

Meshref, W.M., 1990, Tectonic Framework, *in* Said, R., ed., The Geology of Egypt: Rotterdam/Brookfield, Balkema, p. 113-155.

Morgan, P., 1990, Egypt in the framework of global tectonics, *in* Said, R., ed., The Geology of Egypt: Rotterdam/Brookfield, Balkema, p. 91-111.

Omar, G.I., and Steckler, M.S., 1995, Fission Track Evidence on the Initial Rifting of the Red Sea: Two Pulses, No Propagation: Science, v. 270, p. 1341-1344.

Rodi, W., and Mackie, R.L., 2001, Nonlinear conjugate gradients algorithm for 2-D magnetotelluric inversion: Geophysics, v. 66, p. 174-187.

Said, R., 1981, The geological evolution of the River Nile: New York, Springer-Verlag, p. 151 p.

—, 1993, TheRiver Nile: Geology, Hydrology, and Utilization: Oxford/New York, Pergamon, p. 320.

Schumm, S.A., Dumont, J.F., and Holbrook, J.M., 2000, Active tectonics and alluvial rivers: Cambridge; New York, Cambridge University Press, p. 276.

Stern, R.J., and Abdelsalam, M.G., 1996, The Origin of the Great Bend of the Nile from SIR-C/X-SAR Imagery: Science, v. 274, p. 1696-1698.

Tawardros, E., 2001, Geology of Egypt and Libya: Rotterdam/Brookfield, Balkema, p. 468.

Telford, W.M., Geldart, L.P., and Sheriff, R.E., 1990, Applied geophysics: Cambridge/New York, Cambridge University Press, p. 770.

Thurmond, A.K., Stern, R.J., Abdelsalam, M.G., Nielsen, K.C., Abdeen, M.M., and Hinz, E., 2004, The Nubian Swell: Journal of African Earth Sciences, v. 39, p. 401-407.

Vozoff, K., 1991, The magnetotelluric method, *in* Naibighian, M.N., ed., Electromagnetic methods in applied geophysics: Tulsa, Society of Exploration Geophysicists.

Wendorf, F., and Schild, R., 1976, Prehistory of the Nile Valley: New York, Academic Press, p. 404.

Youssef, M.I., 1968, Structural pattern of Egypt and its interpretation: AAPG Bulletin, v. 52, p. 601-614.

Youssef, M.M., 2003, Structural setting of central and south Egypt: An overview: Micropaleontology, v. 49, p. 1-13.

APPPENDICES

Appendix I

Table 1: Gravity Data for Profile 1

Stn. #	UTM N	UTM E	Elevation	Raw Gravity Reading	Lattitude Correction	Free Air Correction	Bouguer Correction	Bouguer Anomaly
1	2682926	477850	168.621	2370.376	0.015	6.749	-2.447	2374.692
2	2682926	477877	167.538	2370.648	0.015	6.414	-2.326	2374.751
3	2682928	477969	164.464	2371.396	0.014	5.465	-1.982	2374.893
4	2682919	478080	167.144	2370.763	0.020	6.292	-2.282	2374.792
5	2682918	478178	170.949	2369.900	0.020	7.466	-2.708	2374.678
6	2682929	478290	166.869	2370.802	0.013	6.207	-2.251	2374.771
7	2682928	478377	163.548	2371.610	0.014	5.182	-1.880	2374.927
8	2682926	478476	162.235	2371.880	0.015	4.780	-1.733	2374.940
9	2682931	478588	155.858	2373.516	0.012	2.809	-1.019	2375.318
10	2682952	478701	150.274	2374.823	-0.001	1.086	-0.394	2375.514
Base	2682951	478812	146.755	2375.612	0.000	0.000	0.000	2375.612
11	2683012	478872	144.337	2376.203	-0.037	-0.746	0.271	2375.690
12	2683064	478968	144.572	2376.289	-0.069	-0.674	0.244	2375.791
13	2683121	479063	146.654	2376.028	-0.103	-0.031	0.011	2375.905
14	2683146	479165	137.763	2378.073	-0.119	-2.775	1.006	2376.186
15	2683163	479212	131.396	2379.223	-0.129	-4.740	1.719	2376.073
16	2683172	479261	129.663	2379.454	-0.134	-5.275	1.913	2375.958
17	2683169	479361	128.16	2379.467	0.133	-5.738	2.081	2375.677
18	2683173	479473	127.212	2379.662	-0.135	-6.031	2.187	2375.683
19	2683177	479560	127.334	2379.843	-0.137	-5.993	2.174	2375.886
20	2683186	479663	126.461	2380.499	-0.143	-6.263	2.271	2376.365
21	2683187	479732	125.53	2380.696	-0.144	-6.550	2.376	2376.378
22	2683182	479761	125.141	2380.672	-0.141	-6.670	2.419	2376.281
23	2683175	479863	123.28	2380.715	-0.136	-7.244	2.627	2375.962
24	2683178	479962	121.975	2380.658	-0.138	-7.647	2.774	2375.646
25	2683165	480062	120.209	2380.753	-0.130	-8.192	2.971	2375.402
26	2683174	480161	118.92	2380.646	-0.136	-8.590	3.115	2375.036
27	2683180	480187	118.894	2380.532	-0.139	-8.598	3.118	2374.913

28	2683160	480266	117.977	2380.48	-0.127	-8.881	3.221	2374.693
29	2683171	480365	117.518	2380.218	-0.134	-9.023	3.272	2374.334
30	2683200	480463	117.044	2379.959	-0.151	-9.169	3.325	2373.964
31	2683168	480657	117.943	2379.27	-0.132	-8.891	3.225	2373.471
32	2683168	480657	117.943	2379.16	-0.132	-8.891	3.225	2373.361
33	2683168	480759	119.135	2378.737	-0.132	-8.524	3.091	2373.173
34	2683173	480860	119.953	2378.348	-0.135	-8.271	3.000	2372.942
35	2683172	480985	120.71	2377.947	-0.134	-8.037	2.915	2372.690
36	2683189	481060	121.352	2377.794	-0.145	-7.839	2.843	2372.653
37	2683187	481111	121.712	2377.573	0.144	7.728	2.803	2372.504
38	2683180	481209	121.477	2377.898	-0.139	-7.801	2.829	2372.787
39	2683169	481248	121.898	2377.902	-0.133	-7.671	2.782	2372.881
40	2683172	481310	122.18	2377.943	-0.134	-7.584	2.751	2372.975
41	2683167	481409	122.694	2378.089	-0.131	-7.425	2.693	2373.225
42	2683165	481483	123.511	2378.083	-0.130	-7.170	2.602	2373.381
43	2683176	481533	124.163	2378.151	-0.137	-6.972	2.529	2373.571
44	2683191	481629	125.203	2378.170	-0.146	-6.651	2.412	2373.785
45	2683187	481703	126.066	2378.099	-0.144	-6.385	2.316	2373.886
46	2683202	481755	126.777	2378.084	-0.153	-6.165	2.236	2374.002
47	2683235	481853	127.643	2378.073	-0.173	-5.898	2.139	2374.141
48	2683240	481942	128.621	2378.162	-0.176	-5.596	2.030	2374.420
49	2683254	481992	128.871	2378.281	-0.184	-5.519	2.002	2374.579
50	2683283	482146	128.699	2378.933	-0.202	-5.572	2.021	2375.180
51	2683320	482199	129.586	2379.185	-0.224	-5.298	1.922	2375.584
52	2683339	482295	133.457	2378.804	-0.236	-4.104	1.488	2375.953
53	2683446	482420	147.249	2376.113	-0.301	0.152	-0.055	2375.909
54	2683535	482511	154.901	2374.576	-0.355	2.514	-0.912	2375.823
55	2683563	482790	155.048	2374.918	-0.372	2.559	0.928	2376.177
56	2683583	482835	154.057	2375.229	-0.384	2.253	-0.817	2376.281
57	2683676	482918	158.396	2374.455	0.441	3.592	1.303	2376.303
58	2683771	483017	164.721	2373.214	-0.499	5.544	-2.011	2376.249
59	2683795	483046	165.173	2373.142	-0.513	5.684	-2.061	2376.251
60	2683874	483132	174.317	2371.183	-0.561	8.506	-3.085	2376.042
61	2683968	483168	174.666	2371.297	-0.619	8.613	-3.124	2376.168

Appendix II

Table 2: Density measurements of Umm Barmil samples.

Sample	Weight (g)	Volume (mL)	Density (g/mL)
1	9.78	4.00	2.445
2	14.44	6.00	2.406666667
3	7.04	2.30	3.060869565
4	15.10	5.10	2.960784314
5	11.38	4.10	2.775609756
6	10.04	4.00	2.51
7	11.78	4.00	2.945
8	12.31	4.20	2.930952381
9	11.56	5.00	2.312
10	7.71	2.90	2.65862069
11	7.25	2.70	2.685185185
12	9.78	3.10	3.15483871
13	7.35	2.90	2.534482759
14	6.69	2.60	2.573076923
15	11.79	4.60	2.563043478
16	10.95	4.00	2.7375
17	8.14	3.30	2.466666667
18	5.68	2.00	2.84
19	6.75	2.80	2.410714286
20	8.52	3.00	2.84
21	6.59	2.80	2.353571429
22	10.73	4.20	2.554761905
23	10.89	4.20	2.592857143
24	7.17	2.70	2.655555556
25	9.32	3.60	2.588888889
26	4.45	1.50	2.966666667
27	7.51	2.40	3.129166667
		Average =	**2.690832579**
	Standard Deviation =		**0.242167**
Relative Standard Deviation =			**8.999723**

Table 3: Density measurements of Timsah samples.

Sample	Weight (g)	Volume (mL)	Density (g/mL)
1	12.91	5.50	2.347272727
2	10.13	4.00	2.5325
3	10.66	4.80	2.220833333
4	11.32	5.00	2.264

5	7.61	3.40	2.238235294
6	10.32	4.00	2.58
7	11.28	5.10	2.211764706
8	9.85	4.20	2.345238095
9	14.56	6.00	2.426666667
10	10.90	4.90	2.224489796
11	6.23	2.40	2.595833333
12	11.02	4.50	2.448888889
13	12.84	5.00	2.568
14	10.82	4.20	2.576190476
15	5.83	2.50	2.332
16	6.76	3.00	2.253333333
17	9.29	4.00	2.3225
18	18.79	7.60	2.472368421
19	8.87	3.80	2.334210526
		Average =	**2.383911874**
	Standard Deviation =		**0.136676**
Relative Standard Deviation =			**5.733251**

Table 4: Density measurements of Abu Aggag samples.

Sample	Weight (g)	Volume (mL)	Density (g/mL)
1	7.72	4.00	1.93
2	6.40	3.00	2.133333333
3	3.51	1.30	2.7
4	4.08	1.50	2.72
5	7.09	4.00	1.7725
6	16.36	12.60	1.298412698
7	8.53	4.00	2.1325
8	5.37	2.60	2.065384615
9	10.75	5.00	2.15
10	10.15	4.80	2.114583333
11	7.01	3.30	2.124242424
12	4.89	2.00	2.445
		Average =	**2.132163034**
	Standard Deviation =		**0.385696**
Relative Standard Deviation =			**18.08943**

Table 5: Density measurements of Precambrian basement samples.

Sample	Weight (g)	Volume (mL)	Density (g/mL)
1	11.13	4.00	2.7825
2	11.52	4.00	2.88
3	19.48	7.50	2.597333333
4	16.03	6.00	2.671666667
5	17.7	7.00	2.528571429
6	19.36	7.50	2.581333333
7	8.34	3.20	2.60625
8	17.48	7.00	2.497142857
9	12.09	4.50	2.686666667
10	12.42	5.00	2.484
11	16.85	6.80	2.477941176
		Average =	**2.617582315**
	Standard Deviation =		**0.128602**
Relative Standard Deviation =			**4.912989**

Appendix III

Table 6: Gravity data acquired along Profile 2.

Stn. #	UTM N	UTM E	Elevation	Raw Gravity Reading	Lattitude Correction	Free Air Correction	Bouguer Correction	Bouguer Anomaly
1	2680127	480073	154.2	2370.175	1.718	2.298	-0.833	2373.357
2	2680342	480200	157.2	2370.737	1.587	3.223	-1.169	2374.378
3	2680468	480330	158.9	2371.655	1.510	3.748	-1.359	2375.554
4	2680593	480471	161.9	2371.285	1.434	4.674	-1.695	2375.698
5	2680716	480747	153.7	2372.506	1.360	2.143	-0.777	2375.232
6	2680845	480733	143.5	2374.525	1.281	-1.004	0.364	2375.166
7	2680928	480798	135.2	2376.236	1.231	-3.566	1.293	2375.194
8	2680984	480866	129.0	2377.558	1.197	-5.479	1.987	2375.263
9	2681045	480945	112.0	2379.047	1.159	-10.725	3.890	2373.371
10	2681109	481021	116.0	2379.605	1.121	-9.491	3.442	2374.677
11	2681174	481092	111.8	2379.384	1.081	-10.787	3.912	2373.590
12	2681245	481163	113.1	2379.151	1.038	-10.386	3.767	2373.570
13	2681309	481239	110.0	2378.912	0.999	-11.343	4.114	2372.682
14	2681373	481312	110.6	2379.017	0.960	-11.157	4.047	2372.866
15	2681441	481386	108.2	2379.451	0.919	-11.898	4.315	2372.787
16	2681512	481459	104.3	2379.902	0.875	-13.102	4.752	2372.428
17	2681582	481530	106.6	2379.722	0.833	-12.392	4.494	2372.657
18	2681650	481595	105.8	2379.751	0.791	-12.639	4.584	2372.488
19	2681717	481668	102.2	2379.240	0.751	-13.750	4.987	2371.228
20	2681782	481747	104.7	2379.237	0.711	-12.978	4.707	2371.677
21	2681816	481781	105.5	2379.223	0.690	-12.731	4.618	2371.800
22	2681853	481818	104.4	2379.174	0.668	-13.071	4.741	2371.512
23	2681917	481894	103.4	2379.238	0.629	-13.379	4.853	2371.340
24	2681985	481964	105.4	2379.320	0.588	-12.762	4.629	2371.774

25	2682046	482041	107.7	2379.566	0.551	-12.052	4.371	2372.435
26	2682108	482111	107.4	2379.189	0.513	-12.145	4.405	2371.962
27	2682141	482148	112.4	2378.881	0.493	-10.602	3.845	2372.617
28	2682175	482187	113.0	2378.504	0.472	-10.417	3.778	2372.337
29	2682240	482261	119.7	2377.469	0.433	-8.350	3.028	2372.581
30	2682310	482337	124.3	2376.826	0.390	-6.930	2.513	2372.800
31	2682378	482399	127.3	2376.224	0.349	-6.004	2.178	2372.746
32	2682436	482481	137.2	2374.782	0.313	-2.949	1.069	2373.216
33	2682494	482554	128.3	2376.201	0.278	-5.695	2.066	2372.849
34	2682559	482631	135.8	2376.653	0.238	-3.381	1.226	2374.737
35	2682611	482707	130.5	2376.619	0.207	-5.016	1.819	2373.629
36	2682685	482777	133.7	2377.717	0.162	-4.029	1.461	2375.311
37	2682746	482856	138.6	2376.586	0.125	-2.517	0.913	2375.107
38	2682802	482910	137.7	2377.669	0.091	-2.794	1.013	2375.979
39	2682885	482978	141.5	2376.408	0.040	-1.622	0.588	2375.415
40	2682943	483046	143.6	2376.508	0.005	-0.974	0.353	2375.892
41	2683004	483108	136.3	2377.308	-0.032	-3.226	1.170	2375.220
42	2683066	483161	151.8	2376.889	-0.070	1.557	-0.565	2377.811
43	2683127	483212	147.0	2376.513	-0.107	0.076	-0.027	2376.454
44	2683179	483288	146.3	2375.592	-0.139	-0.140	0.051	2375.364
45	2683238	483350	140.4	2376.784	-0.175	-1.961	0.711	2375.360
46	2683299	483424	144.3	2376.530	-0.212	-0.758	0.275	2375.835
47	2683364	483492	141.5	2376.837	-0.251	-1.622	0.588	2375.552
48	2683428	483559	141.7	2376.580	-0.290	-1.560	0.566	2375.296

VITA

Jeffrey Dale Roden

Candidate for the Degree of

Master of Science

Thesis: STRUCTURAL INFLUENCE ON THE EVOLUTION OF A PRE-EONILE DRAINAGE SYSTEM OF SOUTHERN EGYPT: INSIGHTS FROM MAGNETOTELLURICS AND GRAVITY DATA

Major Field: Geology

Biographical:

Education:

Completed the requirements for the Master of Science in Geology at Oklahoma State University, Stillwater, Oklahoma in May, 2011.

Completed the requirements for the Bachelor of Science in Geology at Oklahoma State University, Stillwater, Oklahoma in 2007.

Experience:

Geology intern at Kirpatrick Oil Company, Oklahoma City, Oklahoma
Associate Geologist at Territory Resources, Stillwater, Oklahoma

Professional Memberships:
Treasurer of Oklahoma State University Geological Society
Student member of America Association of Petroleum Geologists
Student member of American Geophysical Union
Student member of The Geological Society of America

Name: Jeffrey Dale Roden Date of Degree May, 2011

Institution: Oklahoma State University Location: Stillwater, Oklahoma

Title of Study: STRUCTURAL INFLUENCE ON THE EVOLUTION OF A PRE-EONILE DRAINAGE SYSTEM OF SOUTHERN EGYPT: INSIGHTS FROM MAGNETOTELLURICS AND GRAVITY DATA

Pages in Study: 57 Candidate for the Degree of Master of Science

Major Field: Geology

Scope and Method of Study: Magnetotelluric and gravity surveys were conducted across the Wadi Kobbania in the Western Desert north of Aswan, Egypt. The Wadi Kobbania has been interpreted as the downstream continuation of the Wadi Abu Subeira, comprising an ancient western and northwestern flowing river system, which was sourced from uplifting of the Precambrian Red Sea Hills that occurred during the Oligocene in association with opening of the Red Sea. The purpose of the geophysical surveys was to determine the extent of regional tectonics and local structures on controlling the evolution of the pre-Eonile drainage system predating the modern Nile River. 2D inversion of MT data and gravity models indicate the Wadi Kobbania is filled with loosely-consolidated sedimentary rocks that extend to a depth of ~150-200 m into the Cretaceous sandstone formations which overlie Precambrian crystalline rocks.

Findings and Conclusions: These results were evaluated by two end member models. One model was an incision model in which the wadi was carved into the bedrock. The second is a structural model in which the wadi is considered to represent a graben that was formed by normal faults that deformed the Cretaceous sandstone formations. Geological considerations as well as gravity, MT, and seismic data favors the interpretation that the Wadi Kobbania is a NW trending graben similar to other graben structures that are found as far northwest as 500 km along strike of Wadi Kobbania. These structures are parallel to the western shorelines of the Red Sea and the Gulf of Suez suggesting a regional tectonic link between these extensional structures. Strain localization on faults within the Precambrian crystalline rocks is suggested by the narrow width of the graben, amount of subsidence observed from cross-sectional models, and lack of other known NW trending grabens in the area.

Name: Jeffrey Dale Roden Date of Degree: May, 2011

Institution: Oklahoma State University Location: Stillwater, Oklahoma

ADVISER'S APPROVAL: Dr. Estella Atekwana